Journal of Offshore Mechanics and Arctic Engineering. Received March 29, 2022;
Accepted manuscript posted November 30, 2022. doi:10.1115/1.4056419
Copyright © 2022 by ASME

UiS Subsea-Freight Glider: A Large Buoyancy-Driven Autonomous Cargo Glider

Usman Nawaz Ahmad
University of Stavanger
Stavanger, Norway

Yihan Xing[1]
University of Stavanger
Stavanger, Norway

Yucong Ma
University of Stavanger
Stavanger, Norway

ABSTRACT

This work presents the baseline design for the autonomous subsea vehicle capable of travelling at a lower speed of 1 m/s with an operating range of 400 km. Owing to UiS subsea-freight glider's (USFG) exceedingly economical and unique propulsion system, it can transport various types of cargo over variable distances. The primary use-case scenario for the USFG is to serve as an autonomous transport vessel to carry CO_2 from land-based facilities to subsea injection sites. This allows the USFG to serve as a substitute for weather-dependent cargo tankers and underwater pipelines. The length of the USFG is 50.25 m along with a beam of 5.50 m, which allows the vessel to carry 518 m^3 of CO_2 while serving the storage needs of the carbon capture and storage (CCS) ventures on the Norwegian continental shelf. The USFG is powered by battery cells, and it only consumes a little less than 8 kW of electrical power.

[1] Corresponding author: yihan.xing@uis.no

Accepted Manuscript Not Copyedited

Downloaded from http://asmedigitalcollection.asme.org/offshoremechanics/article-pdf/doi/10.1115/1.4056419/6954108/omae-22-1049.pdf by Stavanger University user on 07 December 2022

Journal of Offshore Mechanics and Arctic Engineering. Received March 29, 2022;
Accepted manuscript posted November 30, 2022. doi:10.1115/1.4056419
Copyright © 2022 by ASME

Along with the mechanical design of the USFG, the control design is also presented in the final part of the paper. The manoeuvring model of the USFG is presented along with two operational case studies. For this purpose, an LQR and PID-based control system is designed, and a detailed comparison study is also shown in terms of tuning and response characteristics for both controllers.

1 INTRODUCTION AND FRAMEWORK

Pipelines transport most of the oil and gas produced from the offshore platforms to the land-based facilities [1]. Subsea pipe laying technology is well-known and has improved significantly since it was first installed and used during World War II by the United Kingdom [2]. Economic and technical problems induce various limitations on this transportation technology. The primary disadvantage is the installation costs. As for remote fields, these costs can be exceptionally high as they intensify with the increased length of the pipeline. Apart from that, deep-water activities such as pipeline inspection are quite costly and challenging. From a financial outlook, pipeline maintenance entails a complete or fractional shutdown, which is not feasible for marginal oil and gas fields. Tanker ships, specifically shuttle tankers, are frequently utilized [3]. A subsea pipeline is an attractive solution for large offshore fields with higher revenue due to the reduced number of step-outs in the operations [4]. Using shuttle tankers provides enhanced flexibility in various situations, i.e., increased demand, as it can swiftly be deployed to the desired location. As for accidents or any unforeseen events, it is advantageous to use tankers instead of conventional pipelines, as an auxiliary ship can be sent quickly. Though, large tanker operations are weather restricted and dependent. Dynamic loads highly influence them in harsh

Accepted Manuscript Not Copyedited

Downloaded from http://asmedigitalcollection.asme.org/offshoremechanics/article-pdf/doi/10.1115/1.4056419/6954108/omae-22-1049.pdf by Stavanger University user on 07 December 2022

Journal of Offshore Mechanics and Arctic Engineering. Received March 29, 2022;
Accepted manuscript posted November 30, 2022. doi:10.1115/1.4056419
Copyright © 2022 by ASME

weather situations from the environment, such as wind and wave loads. To tackle these potential problems, UiS subsea-freight glider (USFG) (illustrated in Fig 1) was introduced, which is a 531-deadweight tonnage (DWT) underwater glider [5] combining the economy and feasibility of the tanker ships along with the underwater capability of submarines. It also serves as an effective alternative to existing technologies for CO_2 transportation. Moreover, it is expected that the cost per ton of transporting CO_2 is comparable to that of the subsea shuttle tanker (SST) [7] [31].

Fig 1 Illustration of UiS subsea-freight glider.

1.1 Earlier Studies in Autonomous and Underwater Cargo Vessels

In 1989, Henry Stommel [8] presented his work on an autonomous observation system intended to collect ocean data. It consisted of "1000 neutrally buoyant floats formally called Slocums" they moved through the ocean by varying their ballast and steered with

Accepted Manuscript Not Copyedited
Downloaded from http://asmedigitalcollection.asme.org/offshoremechanics/article-pdf/doi/10.1115/1.4056419/6954108/omae-22-1049.pdf by Stavanger University user on 07 December 2022

Journal of Offshore Mechanics and Arctic Engineering. Received March 29, 2022;
Accepted manuscript posted November 30, 2022. doi:10.1115/1.4056419
Copyright © 2022 by ASME

hydrodynamic wings. It was originally named Slocum after Joshua Slocum, the first sailor to sail around the world by himself. The initial concept, as proposed by Stommel, has come a long way from small-scale observation floats to Autonomous Underwater Vehicles (AUVs) such as Manta Ray AUV [9] and Glider AUV [10] from Skandi explorer gliders. However, these AUVs have not been utilized for transporting cargo as they are limited by size and loading capacity. Primary cases of underwater vessels with cargo-carrying capabilities date to the 1970s, where Taylor et al. [11] and Jacobsen [12] presented submarines capable of carrying 20,000 to 420,000 DWT of crude oil in the Arctic region. After that, Jacobsen et al. [13] presented in the year 1983 two enormous submarine tankers with the ability to transport 727,400 and 660,000 DWT of Liquefied Natural Gas (LNG). As a result of the Spinnaker program in the 1990s [14], LSE Ltd. developed the Theseus to carry 660 kg of cable to a distance of 900 km. Recently Equinor [15],[16], proposed an autonomous freight-carrying tanker to transport hydrocarbon along with the necessary tools required for subsea operations and CO_2. Moreover, Ellingsen et al. [16] also proposed a large underwater glider that serves as an efficient method to transport cargo. The hydrodynamic analysis on the Equinor autonomous freight-carrying tanker shows that it has significant lower drag comparing to surface tanker ships [18]-[20]. However, the structural design of such vessels is extremely challenging due to the tremendous hydrostatic loads and manufacture imperfections [17]. Reposed to the previous work, Xing [5],[6] presented to utilize an ultra-efficient freight-carrying glider to transport CO_2 while consuming an average power of 10 kW and studies its burst pressure design. The abovementioned research by Ellingsen et al. and Xing were concept proposals and did not divulge any technical details. This work will cover the critical considerations relating to the

Accepted Manuscript Not Copyedited
Downloaded from http://asmedigitalcollection.asme.org/offshoremechanics/article-pdf/doi/10.1115/1.4056419/6954108/omae-22-1049.pdf by Stavanger University user on 07 December 2022

Journal of Offshore Mechanics and Arctic Engineering. Received March 29, 2022;
Accepted manuscript posted November 30, 2022. doi:10.1115/1.4056419
Copyright © 2022 by ASME

baseline design of the USFG followed by well-defined design specifications, which will remove all the knowledge barriers as previously defined. The authors will extend upon the work presented by Xing [19], and Ma et al. [20],[21].

1.2 The UiS Subsea-Freight Glider (USFG)

The USFG is a novel and unique concept owing to its state-of-the-art propulsion system, which varies buoyancy to generate thrust with large hydrodynamic wings instead of using conventional propulsion methods, which consumes significantly more power. Table 1 presents the critical design parameters of the glider. The path taken by the glider is represented in Figure 2, which is formally known as the equilibrium gliding path, the sawtooth pattern [22].

Table 1. Characteristics of USFG.

Parameter	Value	Unit
Net transport economy	< 0.5	-
Pumping time / cycle	< 5% of half cycle	-
Structural weight	419	ton
Vessel length	50.25	m
Volumetric drag coefficient	0.1	-
Wing area	5	m^2
Horizontal speed	1	m/s

Accepted Manuscript Not Copyedited
Downloaded from http://asmedigitalcollection.asme.org/offshoremechanics/article-pdf/doi/10.1115/1.4056419/6954108/omae-22-1049.pdf by Stavanger University user on 07 December 2022

Journal of Offshore Mechanics and Arctic Engineering. Received March 29, 2022;
Accepted manuscript posted November 30, 2022. doi:10.1115/1.4056419
Copyright © 2022 by ASME

Glide path angle	38	°
Average Power	< 8	kW
Ballast fraction	0.15	%
Ballast pump capacity	2000	m^3/h
Deadweight ton	531	ton
Diving depth	200	m

The USFG sails by utilizing its ballast tanks. This process is illustrated in Figure 2. Initially, the ballast water is pumped out of the tanks. This produces a negative pitch angle (bow heading up) and a positive net buoyancy. As a result, the glider becomes lightweight, consequently producing positive buoyancy. The glider, therefore, ascents with an angle of attack. As a result, the relative velocity between the glider and seawater generates a lift force pointing forward and propels the USFG to move towards its desired direction. Similarly, the vessel's weight can be increased by pumping in ballast, generating negative buoyancy and positive pitch angle, which permits the glider to return to its initial depth while moving ahead, as illustrated in Figure *2*. Propulsion is generated by the hydrodynamic wings, which give rise to lift and drag forces while the glider cycles in this to-and-fro pattern while also moving forward. This process is repeated through the entire mission of the USFG, and it minimizes the energy usage onboard as the pumps only require power to regulate water amongst the tanks.

Accepted Manuscript Not Copyedited

Downloaded from http://asmedigitalcollection.asme.org/offshoremechanics/article-pdf/doi/10.1115/1.4056419/6954108/omae-22-1049.pdf by Stavanger University user on 07 December 2022

Journal of Offshore Mechanics and Arctic Engineering. Received March 29, 2022;
Accepted manuscript posted November 30, 2022. doi:10.1115/1.4056419
Copyright © 2022 by ASME

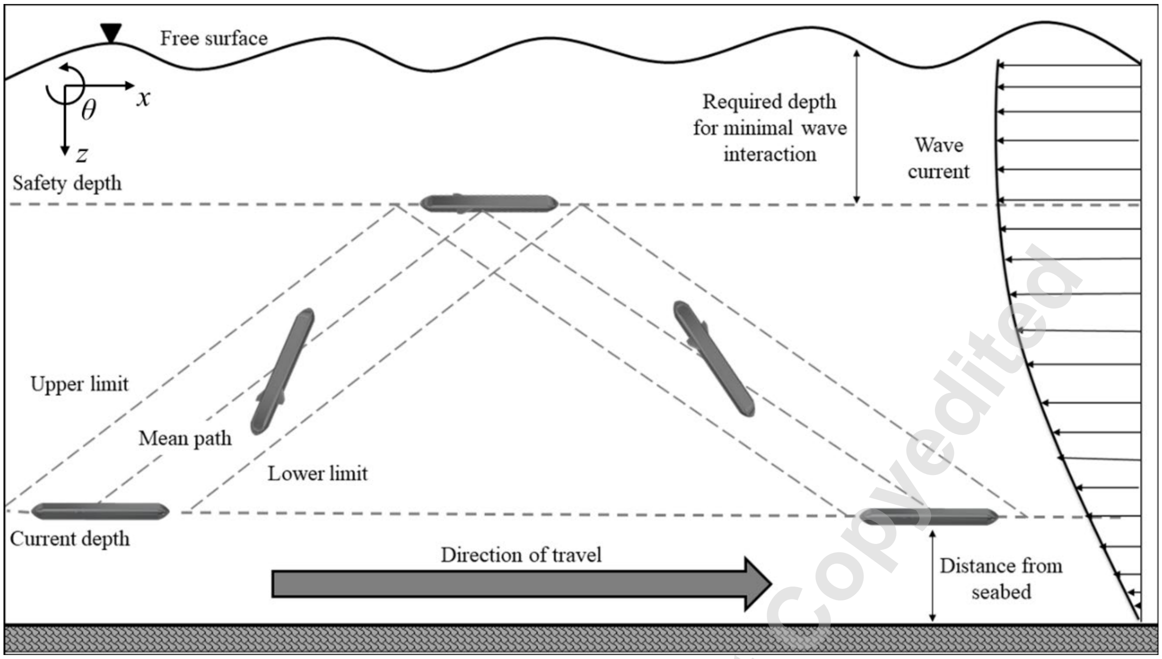

Figure 2 Equilibrium glide paths.

Generally, underwater gliders maneuver in the water by regulating the net buoyancy via changing the ballast volume. At the same time, the roll and the pitch motion of the vessel are controlled by employing a mass actuator. This mechanism is not feasible for large cargo-carrying gliders, as increased size and freight tonnage demand a mammoth actuating and hydraulic network. For the glider dynamics, a swift but robust response system is required to cater to any changes in the operating conditions. The USFG controls the roll and pitch motion with its ailerons combined with varying ballast mass of the tanks to obtain desirable response times, as demonstrated in Figure 3.

Accepted Manuscript Not Copyedited

Downloaded from http://asmedigitalcollection.asme.org/offshoremechanics/article-pdf/doi/10.1115/1.4056419/6954108/omae-22-1049.pdf by Stavanger University user on 07 December 2022

Journal of Offshore Mechanics and Arctic Engineering. Received March 29, 2022;
Accepted manuscript posted November 30, 2022. doi:10.1115/1.4056419
Copyright © 2022 by ASME

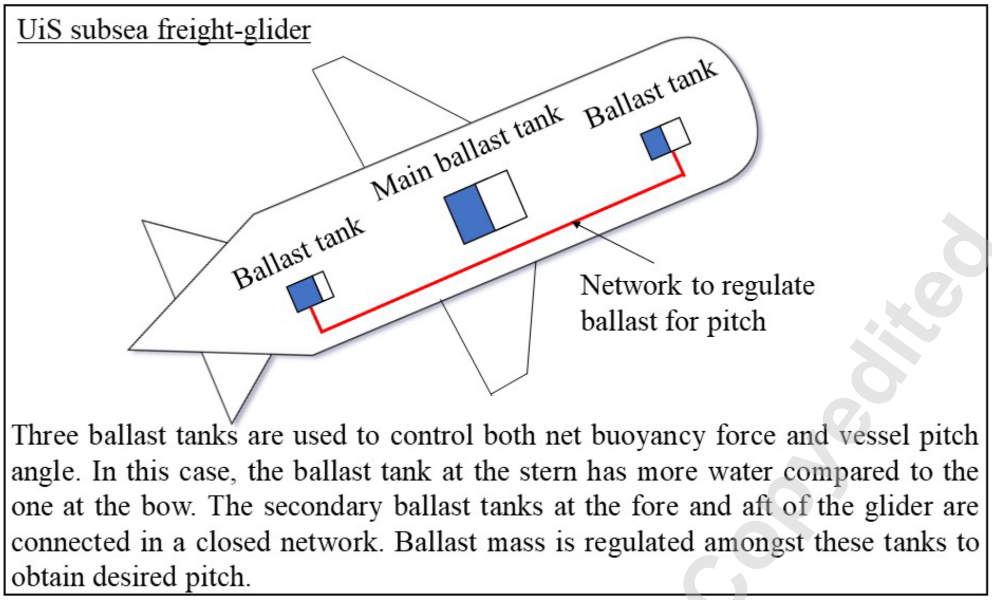

Figure 3 Ballasting system for USFG – top view of the glider.

Two individual proportional-integral-derivative (PID) controllers manage the ballast system on the USFG for pitch and heave motion. A large ballast tank indicated as the main ballast tank in Figure 3 allows the glider to move in the heave direction by controlling the ballast water with a pump onboard. The two secondary ballast tanks located at the fore and aft of the vessel control the pitch angle of the vessel as they are connected in a closed network.

1.3 Use-case Scenario

Figure 4 represents the role of the USFG in the supply chain operations for marine carbon capture and storage (CCS). The USFG is designed to transport CO_2 from land or offshore-based facilities to be injected directly into the seabed using subsea wells. It does so while carrying

Accepted Manuscript Not Copyedited
Downloaded from http://asmedigitalcollection.asme.org/offshoremechanics/article-pdf/doi/10.1115/1.4056419/6954108/omae-22-1049.pdf by Stavanger University user on 07 December 2022

Journal of Offshore Mechanics and Arctic Engineering. Received March 29, 2022;
Accepted manuscript posted November 30, 2022. doi:10.1115/1.4056419
Copyright © 2022 by ASME

out the entire mission autonomously. As the USFG can operate in any climate conditions: it does not restrict its operations in extreme sea states.

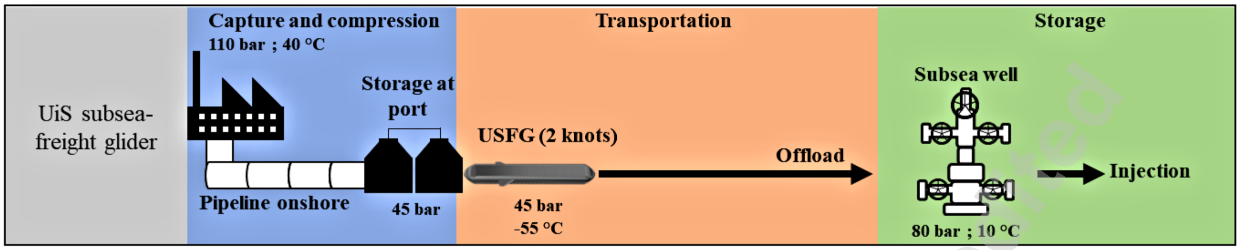

Figure 4 Marine CCS process utilizing USFG.

The baseline design for the glider is planned to be employed in the Norwegian sea CCS projects, Utgard, Snøhvit, and Sleipner offshore fields [23]. These projects involve capturing the CO_2 generated by the oil and gas exploration and production activities while injecting it into the petroleum reservoir. The location of these projects is illustrated in Figure 5. Together with these ventures, Equinor [20] aims to start the Northern Lights Project by 2024, which aims to transport CO_2 generated from land-based industrial activities to be injected into the Utsira formation on the Troll field. The initial design target for the USFG is to be technically feasible for these CCS ventures. Nevertheless, it can easily be configured to be utilized anywhere in various conditions around the globe. Although the study in this work targets CO_2 as the primary cargo but due to its diverse applications, the USFG can also be employed to carry various subsea tools, hydrocarbons, and electricity (by stand-alone battery cells).

Accepted Manuscript Not Copyedited

Downloaded from http://asmedigitalcollection.asme.org/offshoremechanics/article-pdf/doi/10.1115/1.4056419/6954108/omae-22-1049.pdf by Stavanger University user on 07 December 2022

Journal of Offshore Mechanics and Arctic Engineering. Received March 29, 2022;
Accepted manuscript posted November 30, 2022. doi:10.1115/1.4056419
Copyright © 2022 by ASME

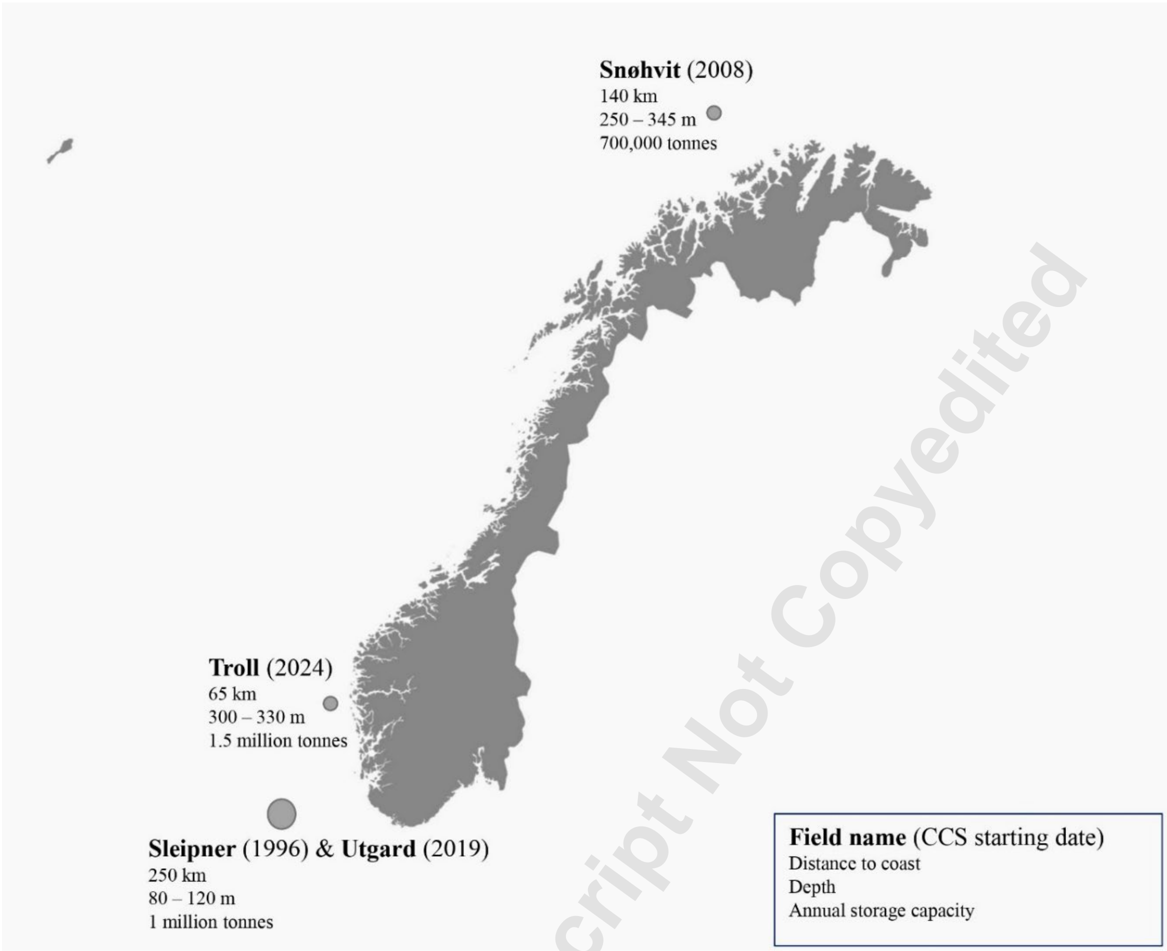

Figure 5 Norwegian sector storage sites for the CCS projects [20].

The USFG can play a vital role in alleviating global warming in several ways. Due to increasing energy demand, the concentration of CO2 in the air is projected to increase two folds by the year 2100 in contrast to the level in 1960 [21]. The CO_2 emissions for transportation activities are zero as the vessel is powered by a battery instead of conventional power sources. This enhances the sustainability value of the shipping industry as it accounts for nearly 3.3% of the hydrocarbon-based CO_2 emissions [26]. Moreover, the vast amount of CO_2 produced from industrial activities worldwide can be captured and stored. This permits the USFG to utilize

Accepted Manuscript Not Copyedited
Downloaded from http://asmedigitalcollection.asme.org/offshoremechanics/article-pdf/doi/10.1115/1.4056419/6954108/omae-22-1049.pdf by Stavanger University user on 07 December 2022

Journal of Offshore Mechanics and Arctic Engineering. Received March 29, 2022;
Accepted manuscript posted November 30, 2022. doi:10.1115/1.4056419
Copyright © 2022 by ASME

small-scale subsea fields as permanent sites for the storage of CO_2, consequently meeting the future requirements of CCS by creating more storage sites [27].

2 BASELINE DESIGN OF THE USFG

The baseline design of USFG is a 531-DWT autonomous glider spanning over a length of 50.25 m with a beam of 5.50 m capable of transporting 518 m^3 of CO_2. It does so while gliding at a 1 m/s (2 knots) with an extended range of 216 nautical miles (400 km).

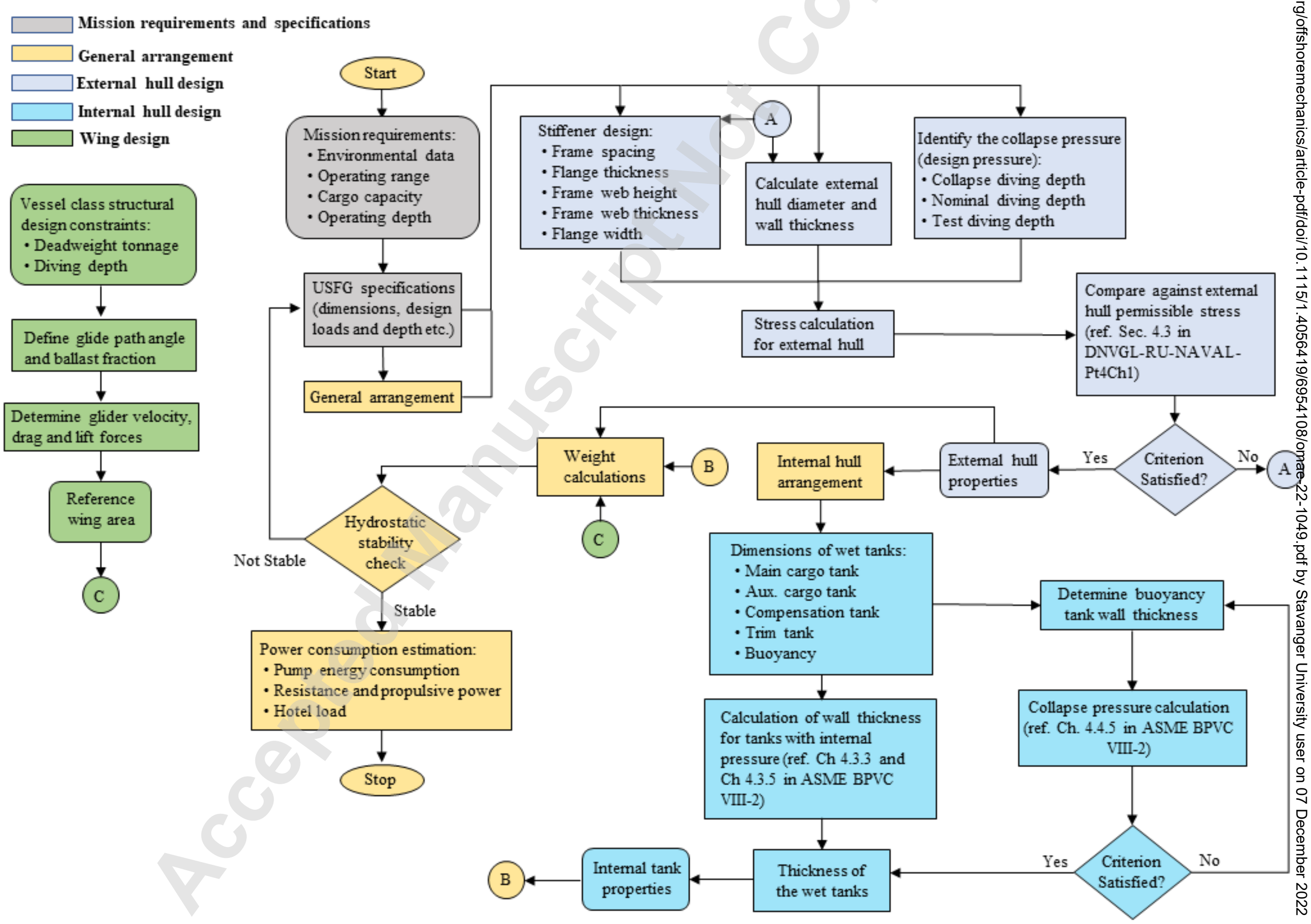

Figure 6 Design flow for USFG baseline design.

Accepted Manuscript Not Copyedited
Downloaded from http://asmedigitalcollection.asme.org/offshoremechanics/article-pdf/doi/10.1115/1.4056419/6954108/omae-22-1049.pdf by Stavanger University user on 07 December 2022

Journal of Offshore Mechanics and Arctic Engineering. Received March 29, 2022;
Accepted manuscript posted November 30, 2022. doi:10.1115/1.4056419
Copyright © 2022 by ASME

This analysis presents the baseline design of the USFG to study this innovative concept and establish its technical and operational limits (if they exist). The mechanical design procedure is highlighted in Figure 6.

As specified by each mission, the assignment requirements serve as an input to the design loop followed by the glider specifications (Section 2.2). It involves the environmental conditions/data, operating range, cargo capacity, and operating depth. Consequently, the USFG specifications are defined: probable load effects, required range, CO_2 cargo properties, and required speed. The general system gives the location and arrangement of all the components of the USFG (Section 2.3). Based on the arrangement and specifications of the USFG, the interior and exterior structural calculations are carried out (Section 2.4). The mechanical design calculations are based on the American Society of Mechanical Engineers Boilers and Pressure Vessel Code (ASME BPVC) VIII-2 [28] and DNV-RU-NAVAL-Pt4CH1 [29], which are the pioneering industrial codes and standards, respectively. The reference area for the wings (Section 2.6) is calculated by the method introduced in Xing et al. [5]. Furthermore, the stability criterion (Section 2.8) is also checked against the hydrostatic properties obtained from the preceding sections. The design loop is an iterative process meaning the dimensions of the glider are adjusted until the stability criterion is not satisfied. Finally, after the final design has been obtained, the amount of power consumed can be obtained (Section 2.9). The extensive details of the design process are in Ma et al. [20].

The aim is to transport a payload that is 50% of the displacement, and it is done by utilizing an Active-Pressure Compensating System (APCS) and a double hull design for the USFG. By employing an APCS, the external loads from the pressure on the external hull can be restricted.

Accepted Manuscript Not Copyedited
Downloaded from http://asmedigitalcollection.asme.org/offshoremechanics/article-pdf/doi/10.1115/1.4056419/6954108/omae-22-1049.pdf by Stavanger University user on 07 December 2022

Journal of Offshore Mechanics and Arctic Engineering. Received March 29, 2022;
Accepted manuscript posted November 30, 2022. doi:10.1115/1.4056419
Copyright © 2022 by ASME

By doing this, the external hull design can be less conservative: as it is not designed to sustain the complete hydrostatic pressure due to the operating water depth. Xing et al. [19] and Ma et al. [20] described this system in more detail. The 50% target is maintained, making the glider economically feasible.

2.1 Mission requirements and USFG Specifications

The mission requirements and the specifications of USFG set the basis for the entire design process. The baseline parameters for the design of USFG are given in Table 2.

Table 2. Design parameters of USFG.

Characteristics	**Value**	**Unit**
Functional depth	200	[m]
Determined range	400	[km]
Operating speed	2	[knots]
Cargo pressure	35 - 55	[bar]
Freight temperature	0 - 20	[°C]
Current velocity	1	[m/s]
Collapse depth	400	[m]

The USFG is designed to carry 531-tons of CO_2 with each trip. It can easily be scaled up to meet the increasing demands of the CCS markets worldwide. Instead of employing a large vessel to carry a huge amount of CO_2 daily, several USFGs can be deployed at the same time to carry the same amount of payload. This can also be a cost-effective solution as the

Accepted Manuscript Not Copyedited
Downloaded from http://asmedigitalcollection.asme.org/offshoremechanics/article-pdf/doi/10.1115/1.4056419/6954108/omae-22-1049.pdf by Stavanger University user on 07 December 2022

Journal of Offshore Mechanics and Arctic Engineering. Received March 29, 2022;
Accepted manuscript posted November 30, 2022. doi:10.1115/1.4056419
Copyright © 2022 by ASME

operations and maintenance costs for smaller vessels are substantial compared to large ones. According to an economic feasibility analysis, the subsea glider is more affordable for those fields with an annual CO_2 capacity of fewer than 1 million tones and less than 500 km from the coast [31].

The operating temperature for the baseline USFG ranges from 0 to 20 °C, which is the range for aquatic ambient temperature. For reference, the temperature in the Norwegian sector (0–10° E, 60–70° N) varies between 2 °C and 12 °C [30]. The design speed for the current is set at 1 m/s; this allows the authors to represent maximum-average current speeds for the Norwegian coast and the North Atlantic region. At the same time, the seasonal normal current speed in the North Sea is observed around 0.2 m/s [32],[33],[34].

To prevent impact from any floating structures or ships on the water's surface, a safety depth of 40 m is defined, which is also illustrated in Figure *2*. This can also minimize the dynamic loads on the USFG from the waves, hence rendering it weather independent. The nominal diving depth is defined based on the retrievable depth from any situations that yield control loss. USFG has a nominal depth of 200 m while transporting CO_2. Thus, the operating depth range of the USFG is between 40 to 200 m. The test diving and collapse depths are 250 m and 400 m, respectively, which are 1.25 and 2.00 times the operating depth and in agreement with Table 1 in DNV-RU-NAVAL-Pt4CH1 [29]. The CCS sites' depth descriptions considered in this work, along with the depths of USFG, are illustrated in Figure 7.

Accepted Manuscript Not Copyedited
Downloaded from http://asmedigitalcollection.asme.org/offshoremechanics/article-pdf/doi/10.1115/1.4056419/6954108/omae-22-1049.pdf by Stavanger University user on 07 December 2022

Journal of Offshore Mechanics and Arctic Engineering. Received March 29, 2022;
Accepted manuscript posted November 30, 2022. doi:10.1115/1.4056419
Copyright © 2022 by ASME

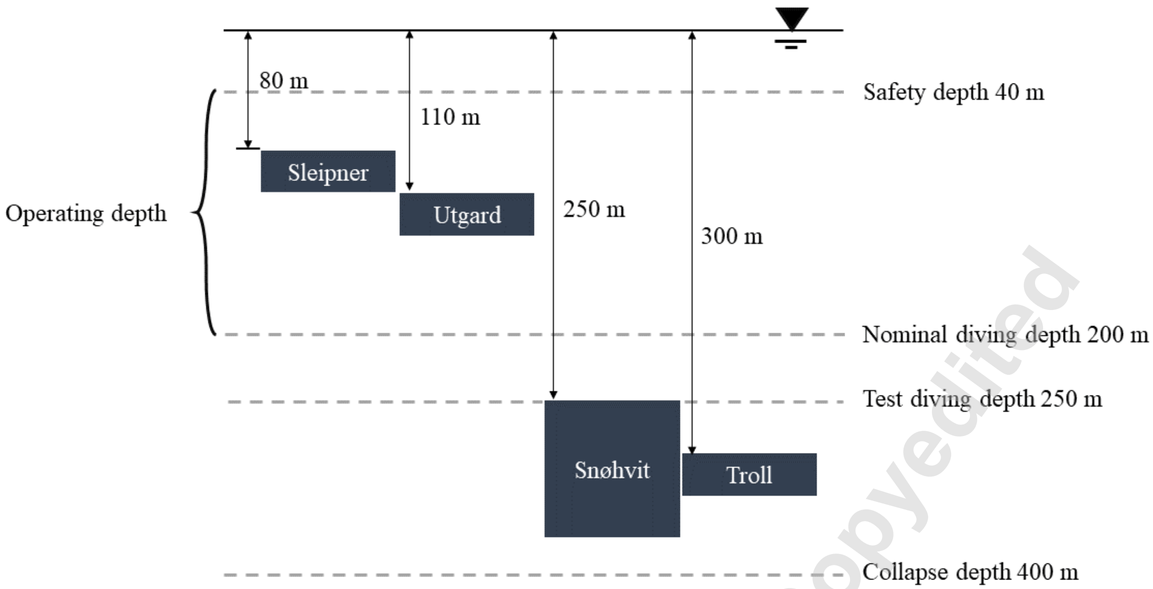

Figure 7 CCS sites depth with USFG depth definitions [20].

The range of USFG, which is 400 km, is designed such that it can complete a one-sided trip to Utgard and Sleipner storage sites. Moreover, a two-way trip can also be accomplished for Troll and Snøhvit fields. For the former case, the USFG can be docked and charged at offshore Utsira High facilities (Gina Krog, Ivar Aasen, and the Edvard Grieg fields) which are powered from the onshore grid with the help of Johan Sverdrup field.

2.2 General Arrangement of the USFG

As shown in Figure 8, the general arrangement drawing depicts the internal tanks and compartments of the external hull.

Accepted Manuscript Not Copyedited
Downloaded from http://asmedigitalcollection.asme.org/offshoremechanics/article-pdf/doi/10.1115/1.4056419/6954108/omae-22-1049.pdf by Stavanger University user on 07 December 2022

Journal of Offshore Mechanics and Arctic Engineering. Received March 29, 2022;
Accepted manuscript posted November 30, 2022. doi:10.1115/1.4056419
Copyright © 2022 by ASME

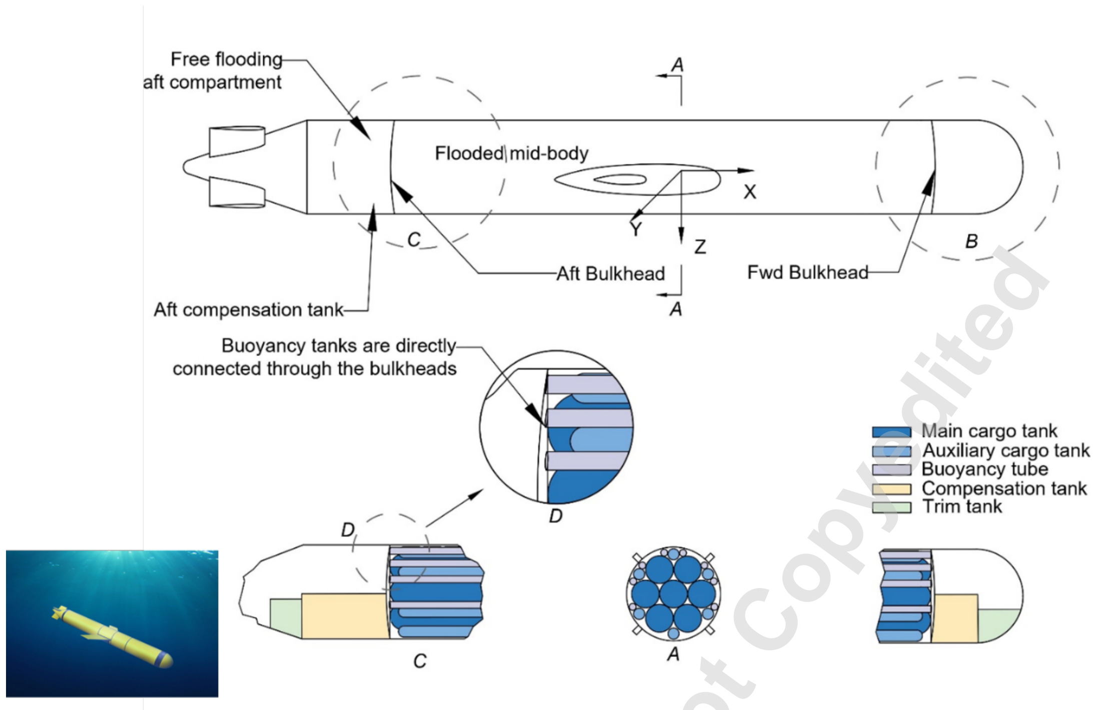

Figure 8 USFG's general arrangement.

To achieve low drag resistance, a torpedo-shaped geometry is employed for the external hull of the USFG. It consists of a cylindrical mid-body, a conical-shaped aft, and a hemispherical designed bow. The aft and the bow sections of the USFG weigh about 23% of the total steel weight, which is used to manufacture the external hull in the baseline USFG. A dual-hull/shell design is employed for the cylindrically formed mid-body to circumvent the design for collapse failure under pressure. The mid-body external hull is free from differential loading, i.e., hydrostatic pressure. The four bulkheads on the USFG are utilized to reinforce the pressure hulls (buoyancy tubes and cargo tanks) and isolate the free-flooded compartment from the mid-body, the flooded section. The buoyancy tubes and the cargo tanks, as illustrated in Figure 8, are the small-scale pressure hulls capable of withstanding collapse and burst pressures.

Accepted Manuscript Not Copyedited
Downloaded from http://asmedigitalcollection.asme.org/offshoremechanics/article-pdf/doi/10.1115/1.4056419/6954108/omae-22-1049.pdf by Stavanger University user on 07 December 2022

Journal of Offshore Mechanics and Arctic Engineering. Received March 29, 2022;
Accepted manuscript posted November 30, 2022. doi:10.1115/1.4056419
Copyright © 2022 by ASME

The external shell or hull of the USFG comprises three different sections: (a) a flooded mid-body in the centre of the vessel which holds piping, buoyancy, and cargo tanks, and it is the largest compartment on the vessel by capacity; (b) a free flooded compartment located at the stern, which encompasses all the equipment that are susceptible to moisture including, rudder controls, gearbox, battery, aft compensation and trim tanks, and motor; (c) a free flooding compartment at the fore which incorporates, the control station, pumps for unloading CO_2, sonar, sensors, fore trim tank, radio, and fore compensation tank. Pressure vessels are an integral part of the USFG, and there are five different kinds of internal pressure vessels onboard, buoyancy tubes, trim tank, main cargo tank, compensation tank, and auxiliary cargo tank.

- *Buoyancy tubes:* To make the USFG neutrally buoyant, eight vacant buoyancy tubes are utilized, which are supported by the bulkheads and have the same span as the main cargo tanks. They are placed at the upper section of the USFG. They are designed to bear collapse pressure.
- *Trim tanks:* There are two trim tanks onboard the USFG, one at the cone in the stern and the other in the fore hemisphere. These tanks aid in achieving a neutral equilibrium position along the length direction. This is done by adjusting the centre-of-gravity (COG) of the vessel directly below the centre-of-buoyancy (COB). Both trim tanks are connected in a closed-loop to regulate the water. Since the tanks are in a flooded mid-body section, they are designed to handle the internal hydrostatic pressure. As a result, they are free from external hydrostatic pressure.

Accepted Manuscript Not Copyedited
Downloaded from http://asmedigitalcollection.asme.org/offshoremechanics/article-pdf/doi/10.1115/1.4056419/6954108/omae-22-1049.pdf by Stavanger University user on 07 December 2022

Journal of Offshore Mechanics and Arctic Engineering. Received March 29, 2022;
Accepted manuscript posted November 30, 2022. doi:10.1115/1.4056419
Copyright © 2022 by ASME

- *Main and supplementary cargo tank:* The USFG has 13 cargo tanks arranged in a rotational symmetry, as shown in Figure *8*, which comprise six auxiliary and seven main cargo tanks. All the cargo tanks have a cylindrical shell and hemispherical heads.
- *Compensation tank:* To provide stability to the USFG, two compensation tanks are used for various hydrostatic loading scenarios. They aim to vary the overall weight of the vessel along with moment (trim) to achieve neutral buoyancy. Compensation tanks along with cargo and trim tanks are designed to withstand burst pressure.

2.3 Structural materials for mechanical design

Materials used in USFG and their graded strength are given in Table 3.

Table 3. USFG's proposed design materials.

Sections	Material	Yield Strength	Tensile Strength
Exterior shell - aft compartment	VL D47	460 MPa	550 MPa
Bulkhead	VL D37	360 MPa	276 MPa
External shell - bow section	VL D47	460 MPa	550 MPa
External shell - mid-body	VL D47	460 MPa	550 MPa
Inner hull - buoyancy tube	SA-738 Grade B	414 MPa	586 MPa
Inner hull - trim tank	SA-738 Grade B	414 MPa	586 MPa
Inner hull - auxiliary cargo tank	SA-738 Grade B	414 MPa	586 MPa

Accepted Manuscript Not Copyedited
Downloaded from http://asmedigitalcollection.asme.org/offshoremechanics/article-pdf/doi/10.1115/1.4056419/6954108/omae-22-1049.pdf by Stavanger University user on 07 December 2022

Journal of Offshore Mechanics and Arctic Engineering. Received March 29, 2022;
Accepted manuscript posted November 30, 2022. doi:10.1115/1.4056419
Copyright © 2022 by ASME

Inner hull - comp. tank	SA-738 Grade B	414 MPa	586 MPa
Internal hull - main cargo tank	SA-738 Grade B	414 MPa	586 MPa

2.4 External shell/hull design

A torpedo-shaped shell is employed for the USFG, having a diameter to length ratio (slenderness ratio) of 1:9.7. This design reduces the manufacturing difficulty of the vessel while optimizing the slenderness of the structure to obtain maximum cargo capacity and reduced drag resistance. The external hull is reinforced by utilizing a stiffener. The properties of the stiffener are highlighted in Table 4. It must be noted that the stiffeners are used conferring to the calculation procedure in DNV-RU-NAVALPt4Ch1 [29], Appendix A, Section 6. The external hulls in the free flooding compartments are subjected to hydrostatic pressures and are checked against permissible stresses at the nominal diving depth, test diving depth, and collapse depth in accordance with Chapter 4 in DNVGL-RU-NAVAL-Pt4Ch1. The permissible values for the stresses are then listed and compared against the criterion to select the stiffener properties, it must be noted that this is an iterative process. Following are the various compartments in the external hull of the USFG.

Table 4 Stiffener properties (external shell).

Elements	Symbol	Units	Value
Inner radius to the flange of the frame	R_f	[mm]	2533
Flange width	b_f	[mm]	80
Frame spacing	L_F	[mm]	1000

Accepted Manuscript Not Copyedited
Downloaded from http://asmedigitalcollection.asme.org/offshoremechanics/article-pdf/doi/10.1115/1.4056419/6954108/omae-22-1049.pdf by Stavanger University user on 07 December 2022

Journal of Offshore Mechanics and Arctic Engineering. Received March 29, 2022;
Accepted manuscript posted November 30, 2022. doi:10.1115/1.4056419
Copyright © 2022 by ASME

Frame cross-sectional area	A_F	[mm^2]	7.35
Flange thickness	s_f	[mm]	30
Frame web height	h_w	[mm]	165
Frame web thickness	s_w	[mm]	30

- The allowable stresses at the collapse, operating, and test diving depths are 415 MPa, 203 MPa, and 418 MPa, respectively.
- Pressure hulls that are designed to withstand hydrostatic pressure are called free flooded compartments. Stresses at various depths (collapse, diving, and test diving) for the compartments are calculated and compared against the allowable stresses in Chapter 4 in DNVGL Rules for Classification for Naval Vessels, Part 4 Sub-surface ships, Section 1 Submarine (DNVGL-RU-NAVAL-Pt4Ch1) [29].
- As stated previously, a similar method is utilized to design a flooded mid-body compartment. Though, this section of the hull does not have to handle the pressure due to the weight of the water on the structure. So, for any accidental or unforeseen load scenarios, namely, vent breakdown, a collapse pressure of 20 bars (200 m) is used to avert instantaneous mechanical or structural failures. Table 5 presents the derived external hull design for USFG. The mid-body accounts for 74 % of the total structural weight, as this section is a substantial part of the baseline USFG design.

Accepted Manuscript Not Copyedited

Downloaded from http://asmedigitalcollection.asme.org/offshoremechanics/article-pdf/doi/10.1115/1.4056419/6954108/omae-22-1049.pdf by Stavanger University user on 07 December 2022

Journal of Offshore Mechanics and Arctic Engineering. Received March 29, 2022;
Accepted manuscript posted November 30, 2022. doi:10.1115/1.4056419
Copyright © 2022 by ASME

292

293 Table 5 USFG's external hull properties.

Sections	Elements	Units	USFG
Free-flooding aft section	Material		VL D47
	Thickness	[m]	0.025
	Design collapse pressure	[bar]	40.000
	Steel Weight	[ton]	15.789
	Length	[m]	10.000
Free-flooding bow section	Material		VL D47
	Thickness	[m]	0.025
	Design collapse pressure	[bar]	40.000
	Steel Weight	[ton]	7.658
	Length	[m]	2.500
Flooded mid-body	Material		VL D47
	Thickness	[m]	0.011
	Design collapse pressure	[bar]	20.000
	Steel Weight	[ton]	66.842
	Length	[m]	37.500

294

Accepted Manuscript Not Copyedited
Downloaded from http://asmedigitalcollection.asme.org/offshoremechanics/article-pdf/doi/10.1115/1.4056419/6954108/omae-22-1049.pdf by Stavanger University user on 07 December 2022

Journal of Offshore Mechanics and Arctic Engineering. Received March 29, 2022;
Accepted manuscript posted November 30, 2022. doi:10.1115/1.4056419
Copyright © 2022 by ASME

2.5 Internal shell/hull design

The internal tanks onboard the USFG are described in this section, and designed per ASME BPVC Chapter 4, Section VIII, Division 2 [28].

- Trim and compensation tanks (free flooded compartments) do not have the requirement to withstand external pressure, making them soft tanks. They are designed to tackle stresses from the hydrostatic pressure (internal pressure) that arises due to the flooded mid-section of the USFG. To obtain a practical sizing parameter for volume and weight, both tanks are assumed to be of cylindrical geometry. The shape of these tanks can be optimized to avail the storage space in the compartment efficiently.
- As for the buoyancy tanks/tubes, the design allows the tubes to endure a 20-bar hydrostatic pressure corresponding to an operating depth of 200 m.
- Cargo tanks that are employed for CO_2 storage are subjected to internal tank pressure and external static pressure from the fluid (water). They have a design burst pressure of 55 bar. This design situation only occurs when the USFG surfaces for routine tasks, such as maintenance, etc. Accordingly, the pressure difference rises to 55 bar because external pressure is 0 bar gauge (barg). An APCS can be utilized to avoid failure due to collapse; extended details can be found in work by Xing et al. [19] and Ma et al. [20].
- Table 6 presents the derived internal tank design for USFG.

Accepted Manuscript Not Copyedited
Downloaded from http://asmedigitalcollection.asme.org/offshoremechanics/article-pdf/doi/10.1115/1.4056419/6954108/omae-22-1049.pdf by Stavanger University user on 07 December 2022

Journal of Offshore Mechanics and Arctic Engineering. Received March 29, 2022;
Accepted manuscript posted November 30, 2022. doi:10.1115/1.4056419
Copyright © 2022 by ASME

315 Table 6 USFG's internal tank characteristics.

Sections	Elements	Units	USFG
Buoyancy Tube (Total tanks = 8)	Material		SA-738 Grade B
	Total volume	[m^3]	25.574
	Acceptable collapse pressure	[bar]	7.000
	Hemispherical end wall thickness	[m]	0.002
	Length	[m]	28.000
	Thickness	[m]	0.004
	Steel weight	[ton]	1.134
	Diameter	[m]	0.390
Auxiliary Cargo Tank (Total tanks = 6)	Material		SA-738 Grade B
	Total volume	[m^3]	67.160
	Acceptable burst pressure	[bar]	55.000
	Hemispherical end wall thickness	[m]	0.008
	Length	[m]	28.000
	Thickness	[m]	0.004
	Steel weight	[ton]	24.322
	Diameter	[m]	0.735
Trim Tank (Total tanks = 2)	Material		SA-738 Grade B
	Total volume	[m^3]	50.000
	Acceptable burst pressure	[bar]	10.000

Accepted Manuscript Not Copyedited

Downloaded from http://asmedigitalcollection.asme.org/offshoremechanics/article-pdf/doi/10.1115/1.4056419/6954108/omae-22-1049.pdf by Stavanger University user on 07 December 2022

Journal of Offshore Mechanics and Arctic Engineering. Received March 29, 2022;
Accepted manuscript posted November 30, 2022. doi:10.1115/1.4056419
Copyright © 2022 by ASME

	Length	[m]	1.890
	Thickness	[m]	0.002
	Steel weight	[ton]	73.705
	Diameter	[m]	3.500
Compensation Tank (Total No.= 2)	Material		SA-738 Grade B
	Total volume	[m^3]	22.96
	Acceptable burst pressure	[bar]	8.000
	Length	[m]	1.750
	Thickness	[m]	0.002
	Steel weight	[ton]	33.561
	Diameter	[m]	3.750
Main Cargo Tank (Total tanks = 7)	Material		SA-738 Grade B
	Total volume	[m^3]	459.366
	Acceptable burst pressure	[bar]	55.000
	Hemispherical end wall thickness	[m]	0.009
	Length	[m]	28.000
	Thickness	[m]	0.017
	Steel weight	[ton]	119.859
	Diameter	[m]	1.500

Accepted Manuscript Not Copyedited
Downloaded from http://asmedigitalcollection.asme.org/offshoremechanics/article-pdf/doi/10.1115/1.4056419/6954108/omae-22-1049.pdf by Stavanger University user on 07 December 2022

Journal of Offshore Mechanics and Arctic Engineering. Received March 29, 2022;
Accepted manuscript posted November 30, 2022. doi:10.1115/1.4056419
Copyright © 2022 by ASME

2.6 Wing design

The design procedure for the wings is highlighted in Figure 9. Glider parameters are defined in Figure 10, with Fb being the buoyancy force and W being the overall weight of the vessel. The vessel class (cargo carrying capacity) is defined along with the nominal operating depth of the USFG, which serves as the basis for selecting an optimal glide path angle. From the gliding angle, velocities of the USFG can be calculated, which further yields drag and lift forces. Lastly, the hydrofoil's reference area and lift to drag ratio can be decided.

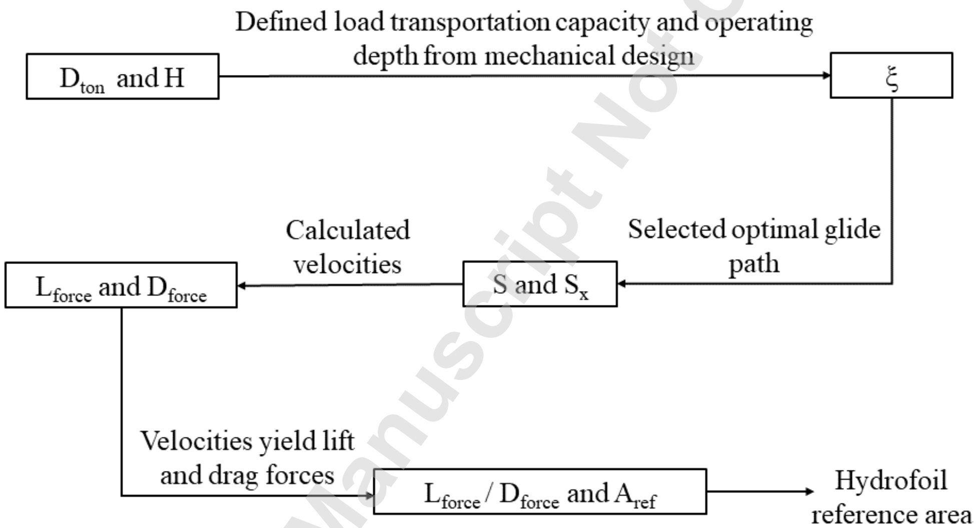

Figure 9 USFG's global parameters.

Downloaded from http://asmedigitalcollection.asme.org/offshoremechanics/article-pdf/doi/10.1115/1.4056419/6954108/omae-22-1049.pdf by Stavanger University user on 07 December 2022
Accepted Manuscript Not Copyedited

Journal of Offshore Mechanics and Arctic Engineering. Received March 29, 2022;
Accepted manuscript posted November 30, 2022. doi:10.1115/1.4056419
Copyright © 2022 by ASME

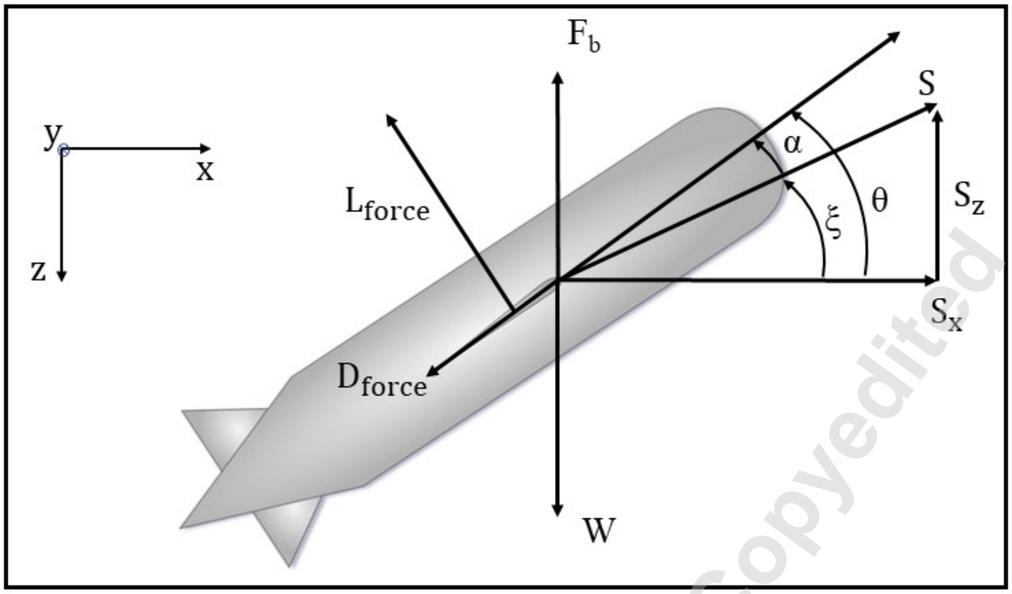

Figure 10 USFG's gliding parameters – side view of the glider.

The hydrofoil reference area comes out to be around 7 m^2 by following this procedure. Detailed calculations and the nomenclature for this section can be found in **Appendix A. Calculation of reference wing area**.

2.7 Weight estimations

After the mechanical design has been finalized (Ref. Section 2.3-2.6), weight calculations (Table 7) for the USFG can be performed. Weight and storage capacity for CO_2-filled scenarios are given in. Subsequent weight definitions are employed to be used in USFG:

- The permanent ballast onboard is 2% of displacement.
- The targeted CO_2 load or payload is 44% of displacement.
- The trim (moment) ballast onboard is 0.5% of displacement.
- The weight of the machinery onboard the vessel is 2% of displacement.

Accepted Manuscript Not Copyedited
Downloaded from http://asmedigitalcollection.asme.org/offshoremechanics/article-pdf/doi/10.1115/1.4056419/6954108/omae-22-1049.pdf by Stavanger University user on 07 December 2022

Journal of Offshore Mechanics and Arctic Engineering. Received March 29, 2022;
Accepted manuscript posted November 30, 2022. doi:10.1115/1.4056419
Copyright © 2022 by ASME

Table 7 USFG's weight configuration (CO_2 charged).

Module	Weight (tons)	
	USFG	
Structure	419	30.42%
Permanent ballast mass	30	2.23%
Freight	612	44.45%
Compensation ballast	51	3.72%
Equipment	30	2.23%
Mid-body seawater	226	16.42%
Trim ballast mass	7	0.52%
Total	**1379**	**100%**

2.8 Hydrostatic stability study

After the weight estimations, criteria for intact stability are checked under DNVGL-RUNAVAL-Pt4Ch1 Section 3.5.2.3. The classification chosen is for submarines with a displacement ranging between 1000-2000 tons [29]. For USFG, the metacentric height (GM) should exceed 0.22 m, and the distance between the centre of gravity (G) and centre of buoyancy (B) must be higher than 0.35 m. This section considers four cases of hydrostatic loading, which are as follows.

1. *Surfaced (SW-filled)*: the USFG is floating on the water's surface, while three out of six auxiliary and five main tanks are filled with heavy seawater/saltwater. All

Accepted Manuscript Not Copyedited
Downloaded from http://asmedigitalcollection.asme.org/offshoremechanics/article-pdf/doi/10.1115/1.4056419/6954108/omae-22-1049.pdf by Stavanger University user on 07 December 2022

Journal of Offshore Mechanics and Arctic Engineering. Received March 29, 2022;
Accepted manuscript posted November 30, 2022. doi:10.1115/1.4056419
Copyright © 2022 by ASME

the remaining tanks aboard the vessel are bare. This scenario is observed at the start and end of the CO_2 transportation cycle when the USFG surfaces to load and unload the cargo, respectively.

2. *Surfaced (CO_2-filled)*: this scenario occurs after the tanks of the USFG are filled with CO_2. At this point, the USFG is ready to dive to the nominal operating depth.
3. *Submerged (CO_2-filled)*: liquid CO_2 is filled in all the 13 cargo tanks (main and auxiliary). At this stage, the USFG is fully submerged and loaded with CO_2.
4. *Submerged (SW-filled)*: this case arises after the USFG has unloaded the CO_2 at the subsea well. The vessel is submerged as the cargo tanks are replaced with seawater during unloading.

Table 8 outlines the results from this section. Finally, extended details for this check can also be found in Xing et al. [7] and Ma et al. [20].

Table 8 Hydrostatic stability study.

	USFG			
	Surfaced (SW-filled)	**Surfaced (CO_2-filled)**	**Submerged (CO_2-filled)**	**Submerged (SW-filled)**
CoG (x, y, z)	[-0.937, 0.00, 0.147]	[-1.032, 0.00, 0.276]	[-0.784, 0.00, 0.403]	[-0.829, 0.00, 0.460]
BG	3.807	5.252	0.405	0.460
CoB (x, y, z)	[-1.481, 0.00, 4.200]	[-1.481, 0.00, 5.500]	[-1.481, 0.00, 0.00]	[-1.481, 0.00, 0.00]
GM	0.393	0.248	0.405	0.460
M (x, y, z)	[0.00, 0.00, 0.00]	[0.00, 0.00, 0.00]	[0.00, 0.00, 0.00]	[0.00, 0.00, 0.00]

Downloaded from http://asmedigitalcollection.asme.org/offshoremechanics/article-pdf/doi/10.1115/1.4056419/6954108/omae-22-1049.pdf by Stavanger University user on 07 December 2022
Accepted Manuscript Not Copyedited

Journal of Offshore Mechanics and Arctic Engineering. Received March 29, 2022;
Accepted manuscript posted November 30, 2022. doi:10.1115/1.4056419
Copyright © 2022 by ASME

Effect	GM > 0.22 == OK	GM > 0.22 == OK	BG > 0.35 == OK	BG > 0.35 == OK

2.9 Power utilization analysis

The amount of power consumed is a function of the glide path (Ref. to ξ in Figure *10*) along with the ballast fraction (BF): the ballast tank size, as the USFG, can vary the speed with which it glides. To better visualize the system's performance, two glide path angles are considered; an angle that gives maximum horizontal velocity for the USFG and a shallower gliding angle.

As the USFG glides faster, it needs to incline at steeper angles while pumping in ballast more frequently to travel the required distance. Shallow glide angles generally result in a comparatively slow equilibrium glide, yielding low horizontal speeds. However, there is an added benefit of utilizing less pumping power/work while travelling a great amount of distance horizontally. As for steep gliding angles, higher horizontal velocity can be achieved by pumping in more ballast water, highlighted by graver [30]. This expands extensive energy on the pump onboard the vessel, leading to more pump work.

With the increase in BF, the horizontal velocity of the USFG also rises. Hence, USFG can be designed to travel much faster by selecting higher BFs. By doing this, the required pumping power will also be considerably increased. A parametric study is done to achieve the optimal BF that limits the pumping work and the pump's size. For each BF, the horizontal glider velocity is calculated and plotted against the consumed power as shown in Figure 11.

Accepted Manuscript Not Copyedited
Downloaded from http://asmedigitalcollection.asme.org/offshoremechanics/article-pdf/doi/10.1115/1.4056419/6954108/omae-22-1049.pdf by Stavanger University user on 07 December 2022

Journal of Offshore Mechanics and Arctic Engineering. Received March 29, 2022;
Accepted manuscript posted November 30, 2022. doi:10.1115/1.4056419
Copyright © 2022 by ASME

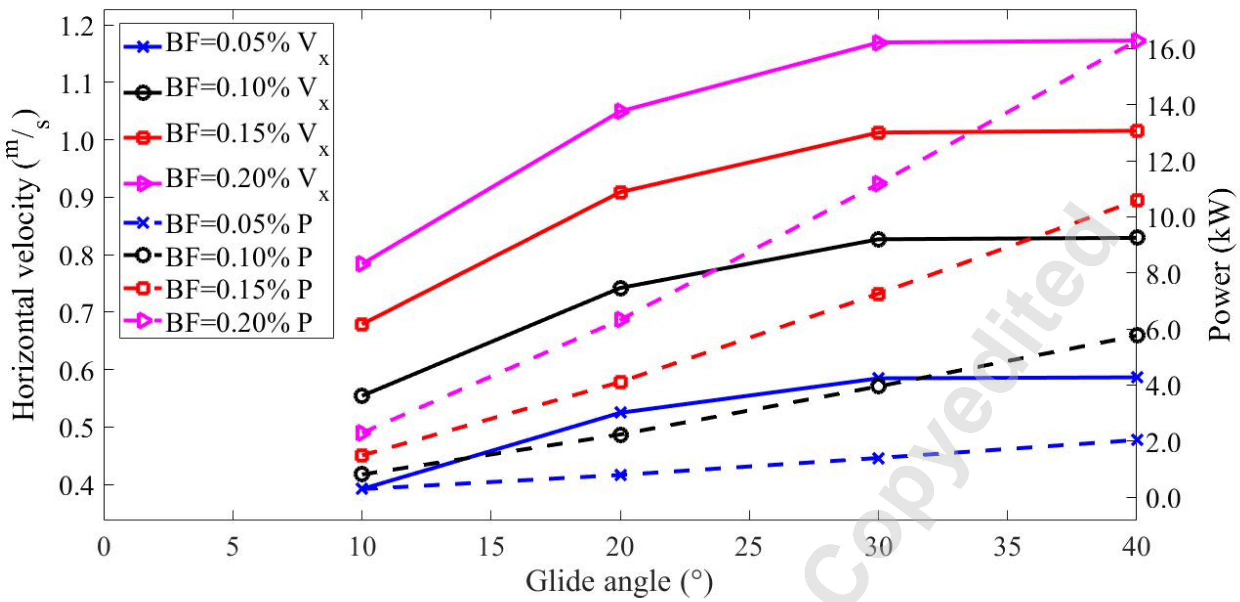

Figure 11 Horizontal velocity vs power consumption.

Depending on the USFG's mission, a desired operational gliding angle must be selected. This is dependent on a quid pro quo between the maximum horizontal glide-velocity and the required pumping work. From Figure 11, a balance between a steep and shallow glide angle must be struck to have an optimal speed and consume minimum power. So, a glide angle of 30° along with a BF of 0.15% is chosen as it caters to the required velocity (1 m/s) of the USFG while consuming a smaller amount of power (<8kW). Lower gliding angles are not considered as they fail to achieve the targeted velocity, even though the power consumption for smaller angles is quite insignificant. As for higher gliding angles, moving from 30° to 40°, the amount of power consumed becomes substantial, and the velocity difference is relatively minimal. Moreover, there is no added advantage of choosing a steeper glide angle than 30° rather than just increasing the pumping work.

Accepted Manuscript Not Copyedited
Downloaded from http://asmedigitalcollection.asme.org/offshoremechanics/article-pdf/doi/10.1115/1.4056419/6954108/omae-22-1049.pdf by Stavanger University user on 07 December 2022

Journal of Offshore Mechanics and Arctic Engineering. Received March 29, 2022;
Accepted manuscript posted November 30, 2022. doi:10.1115/1.4056419
Copyright © 2022 by ASME

3 DYNAMIC RESPONSE OF THE USFG

3.1 Coordinate system

To fully describe and understand the dynamics of the USFG, two-coordinate frames are defined, i.e., body-bound and earth frames. The body-bounded frame (O_b, X_b, Y_b, Z_b) of the USFG is located at its centre-of-gravity (G). Its motion involves a local north, east, and down coordinate system (O_E, X_E, Y_E, Z_E). The centre-of-buoyancy (B) is located accurately above the G and at the geometric centre of the USFG; this ensures enhanced stability of the vessel. The motion and its direction along the six degrees of freedom and the frames are highlighted in Figure 12.

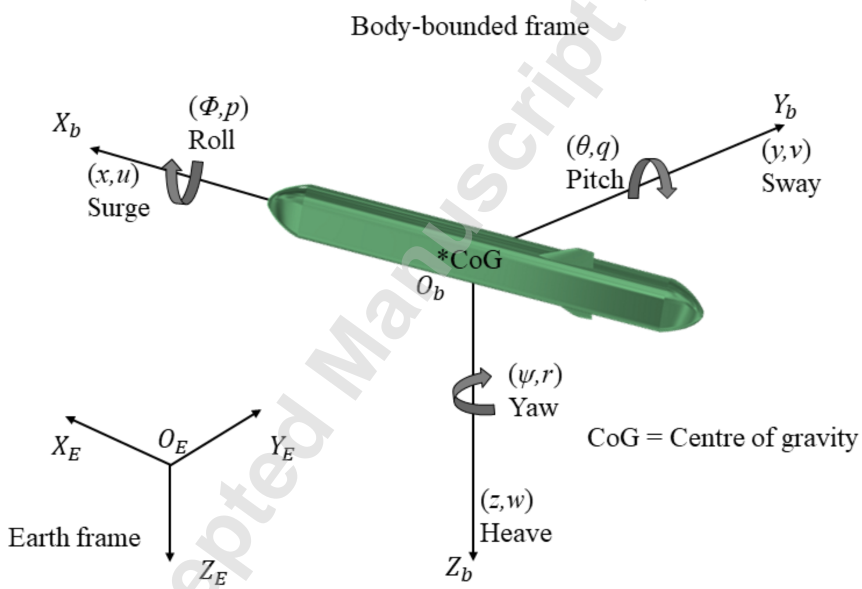

Figure 12 Coordinate system.

Accepted Manuscript Not Copyedited
Downloaded from http://asmedigitalcollection.asme.org/offshoremechanics/article-pdf/doi/10.1115/1.4056419/6954108/omae-22-1049.pdf by Stavanger University user on 07 December 2022

Journal of Offshore Mechanics and Arctic Engineering. Received March 29, 2022;
Accepted manuscript posted November 30, 2022. doi:10.1115/1.4056419
Copyright © 2022 by ASME

3.2 Modeling of USFG

3.2.1 Simulink/Simscape model

SimMechanics is utilized to capture the dynamics of the USFG. Figure 13 (a) presents the control process of the USFG pitch control problem. Figure 13 (b) depicts the corresponding dynamic model of the USFG in the Simscape environment.

Accepted Manuscript Not Copyedited
Downloaded from http://asmedigitalcollection.asme.org/offshoremechanics/article-pdf/doi/10.1115/1.4056419/6954108/omae-22-1049.pdf by Stavanger University user on 07 December 2022

Journal of Offshore Mechanics and Arctic Engineering. Received March 29, 2022;
Accepted manuscript posted November 30, 2022. doi:10.1115/1.4056419
Copyright © 2022 by ASME

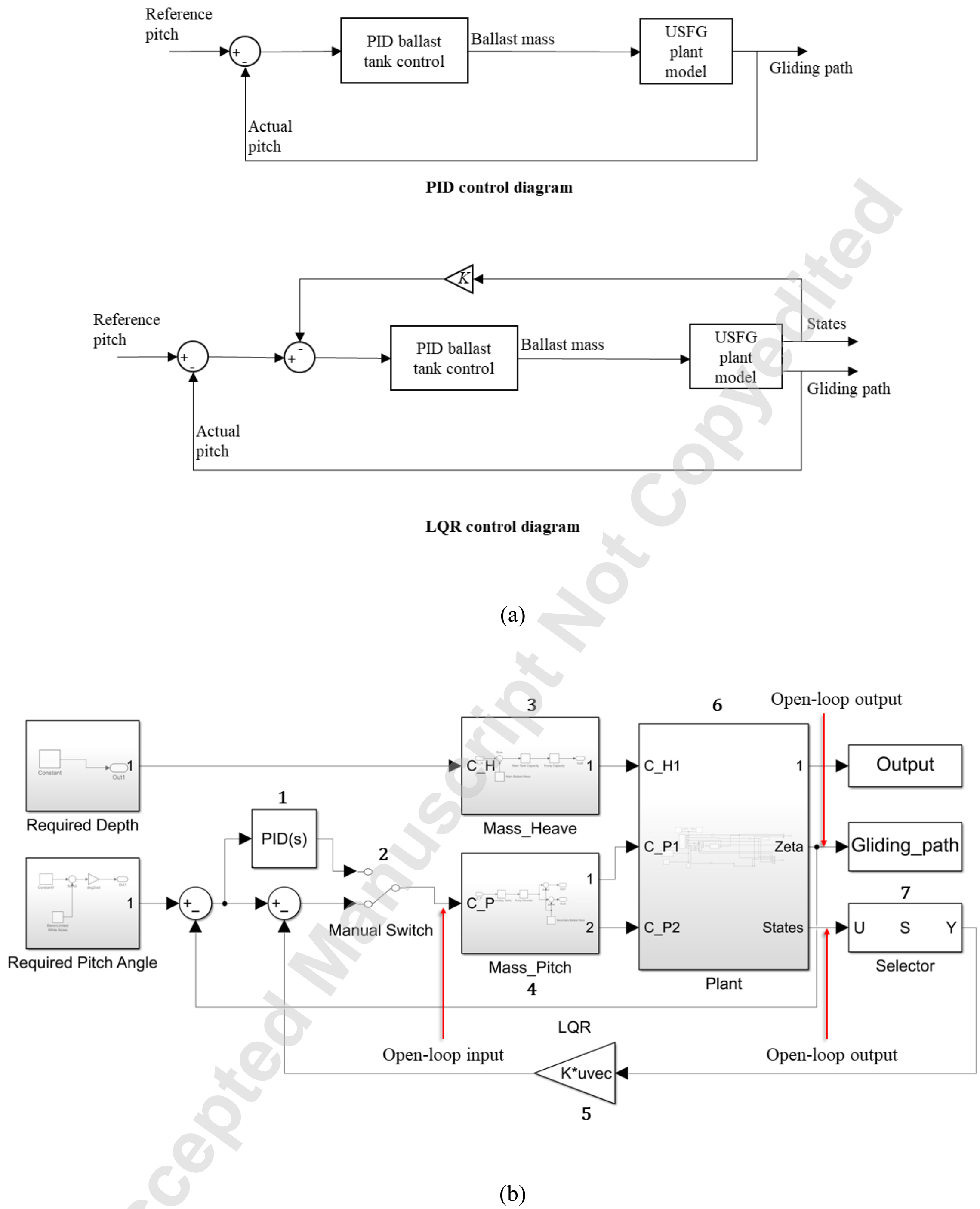

Figure 13 (a) block diagram and (b) mathematical model of the USFG.

The central blocks that are used to model the vessel, as highlighted in Figure 13 are elaborated below.

Accepted Manuscript Not Copyedited
Downloaded from http://asmedigitalcollection.asme.org/offshoremechanics/article-pdf/doi/10.1115/1.4056419/6954108/omae-22-1049.pdf by Stavanger University user on 07 December 2022

Journal of Offshore Mechanics and Arctic Engineering. Received March 29, 2022;
Accepted manuscript posted November 30, 2022. doi:10.1115/1.4056419
Copyright © 2022 by ASME

- *Block no.1:* this is the Proportional-integral-derivative (PID) type control that adjusts the pitch motion of the glider. Moreover, it can also be easily tuned to regulate the heave motion of the vessel.
- *Block no.2:* a manual switch that can direct power between the linear quadratic regulator (LQR) and PID controllers.
- *Block no.3:* termed as the heave block. Its purpose is to vary the ballast mass into the ballast tanks. This allows the glider to travel along the vertical direction with the help of lift and drag forces that are generated owing to its large hydrofoils. A saturation (limits the amount of ballast into the tanks) and a rate-limiter (bounds the volumetric flowrate) block is also confined in this sub-system.
- *Block no.4:* the pitch block that is responsible for varying the ballast among the secondary tanks of the glider. This allows the USFG to pitch forward or backward, depending upon the configuration.
- *Block no.5:* this is the LQR type controller that simply multiplies the gain obtained from system optimization with the states of the system. More details of the controller are discussed in subsequent sections.
- *Block no.6:* the plant block represents the plant model of the glider. This block is discussed briefly in the next section.
- *Block no.7:* This block aims to arrange the state variables in a definite vector. An LQR type control is formed when this vector is multiplied by the gain matrix (K) to form a closed loop.

Accepted Manuscript Not Copyedited
Downloaded from http://asmedigitalcollection.asme.org/offshoremechanics/article-pdf/doi/10.1115/1.4056419/6954108/omae-22-1049.pdf by Stavanger University user on 07 December 2022

Journal of Offshore Mechanics and Arctic Engineering. Received March 29, 2022;
Accepted manuscript posted November 30, 2022. doi:10.1115/1.4056419
Copyright © 2022 by ASME

3.2.2 Plant block/model

This section describes the plant block depicted in Figure 13 as *block no.6*. A systematic configuration of the block is presented in Figure 14 below. The three main blocks that comprise the plant block are as follows:

- *USFG:* this block contains a two-dimensional (2D) rigid body that is allowed to move in three degrees of freedom (*x*, *y*, and *z*). Based on the forces acting on the glider, the following equations of motion will be solved:

$$W(\dot{u} + wq - xq^2 + z\dot{q}) = \sum X_e \quad (1)$$

$$W(\dot{w} + uq - zq^2 + x\dot{q}) = \sum Z_e \quad (2)$$

$$I_{yy}\dot{q} + W\lfloor z(\dot{u} + wq) - x(\dot{w} - uq)\rfloor = \sum M_e \quad (3)$$

Velocities are expressed as u, w, and $\dot{q}$ and similarly acceleration by $\dot{u}$, $\dot{w}$, and $\ddot{q}$ in surge, heave, and pitch directions respectively. Equations (1-3) encompass external forces in pitch (M_e), heave (Z_e), and surge (X_e) as presented on the right-hand side and inertial terms on the other side. This is further highlighted in Figure 14; it must be noted that connection points are marked by dots in the figure.

Accepted Manuscript Not Copyedited
Downloaded from http://asmedigitalcollection.asme.org/offshoremechanics/article-pdf/doi/10.1115/1.4056419/6954108/omae-22-1049.pdf by Stavanger University user on 07 December 2022

Journal of Offshore Mechanics and Arctic Engineering. Received March 29, 2022;
Accepted manuscript posted November 30, 2022. doi:10.1115/1.4056419
Copyright © 2022 by ASME

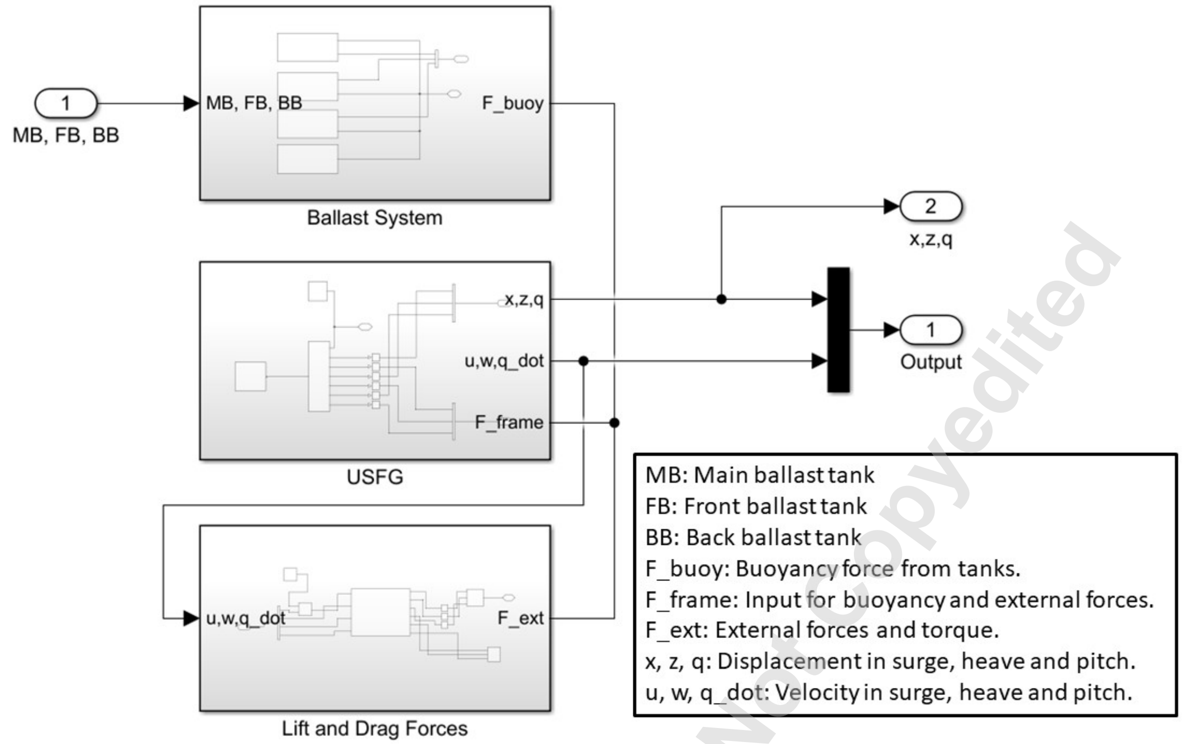

Figure 14 Simulink plant model - Lift and drag forces, ballast system, and USFG.

- *Ballast system:* this block model the dynamics of the actuating mechanism of the USFG. As described earlier, it serves input to the USFG block as a force by taking control of ballast inputs from the mass blocks. Finally, the buoyancy force of the glider is also simulated in this system.
- *Drag and lift force:* drag and lift force and the rotational torque are determined in this block. These are calculated based on the approach angle of the incoming flow. Velocities and the pitching angles of the USFG are utilized to calculate the forces. Equations (4) and (5) are used to calculate the drag and lift coefficients which are a function of approach angle (α) as depicted in Figure *10*. These are the volumetric drag and lift coefficients used by Graver [35], as the shape of the

Downloaded from http://asmedigitalcollection.asme.org/offshoremechanics/article-pdf/doi/10.1115/1.4056419/6954108/omae-22-1049.pdf by Stavanger University user on 07 December 2022
Accepted Manuscript Not Copyedited

Journal of Offshore Mechanics and Arctic Engineering. Received March 29, 2022;
Accepted manuscript posted November 30, 2022. doi:10.1115/1.4056419
Copyright © 2022 by ASME

USFG is similar to the glider proposed in his work. The lift (L_f) and drag (D_f) forces and the rotational torque (M_T) experienced by the USFG are also calculated in the plant model, these are given by equation (6). Where δ_w represents the density of seawater, V_{sub} is the submerged volume of the vessel, and S is the total velocity manoeuvring velocity of the glider. C_L and C_D are the lift and drag coefficients given by equations (4) and (5), respectively, whereas C_{DM} is the damping moment coefficient. The C_{DM} value of 1000 used in this study has been verified and established by utilizing decay tests and is shown to work well for this study. It is noted that this value would need to be obtained via experimental testing for real-life applications.

$$C_L = 5\alpha^2 + 10\alpha \tag{4}$$

$$C_D = 0.4\alpha^2 + \alpha + 0.1 \tag{5}$$

$$\begin{aligned} L_{force} &= \frac{1}{2} \times C_L \times \delta_w \times V_{sub} \times S^2 \\ D_{force} &= \frac{1}{2} \times C_D \times \delta_w \times V_{sub} \times S^2 \\ M_T &= -\frac{1}{2} \times C_{DM} \times \delta_w \times V_{sub} \times q^2 \end{aligned} \tag{6}$$

Accepted Manuscript Not Copyedited

Downloaded from http://asmedigitalcollection.asme.org/offshoremechanics/article-pdf/doi/10.1115/1.4056419/6954108/omae-22-1049.pdf by Stavanger University user on 07 December 2022

Journal of Offshore Mechanics and Arctic Engineering. Received March 29, 2022;
Accepted manuscript posted November 30, 2022. doi:10.1115/1.4056419
Copyright © 2022 by ASME

Similarly, the drag and lift generated by the large hydrofoils are also applied and modeled in this plant model. The reference wing area calculated in Section 2.6 is also combined into this block. NACA 4412 airfoil [35] geometry is employed to capture the dynamics of the USFG's hydrofoils. W_L and W_D are the lift and drag forces generated by the hydrofoils, while W_M is the moment. The modified equations for the hydrofoils are given below:

$$W_L = \frac{1}{2} \times C_{LW} \times \delta_w \times V_{sub} \times S^2$$

$$W_D = \frac{1}{2} \times C_{DW} \times \delta_w \times V_{sub} \times S^2 \qquad (7)$$

$$W_M = -\frac{1}{2} \times C_{DMW} \times \delta_w \times V_{sub} \times q^2$$

C_{LW}, C_{DW}, and C_{DMW} are the modified volumetric coefficients for the hydrofoils, given by equation (8).

$$C_{LW} = a\alpha^3 + b\alpha^2 + c\alpha + d$$

$$a = -10 \times 10^{-5}; b = -9 \times 10^{-4}; c = 0.114; d = 0.4942$$

Accepted Manuscript Not Copyedited
Downloaded from http://asmedigitalcollection.asme.org/offshoremechanics/article-pdf/doi/10.1115/1.4056419/6954108/omae-22-1049.pdf by Stavanger University user on 07 December 2022

Journal of Offshore Mechanics and Arctic Engineering. Received March 29, 2022;
Accepted manuscript posted November 30, 2022. doi:10.1115/1.4056419
Copyright © 2022 by ASME

$$C_{DW} = Ae^{(B\alpha)} + Ce^{(D\alpha)}$$

$$A = 2 \times 10^{-3}; B = -0.2093; C = 2.5 \times 10^{-3}; D = 0.1892 \tag{8}$$

$$C_{DMW} = p + i\cos(\alpha n) + r\sin(\alpha n) + t\cos(2\alpha n) + y\sin(2\alpha n)$$

$$p = -0.085; i = -0.026; r = 0.014; t = 0.0076; y = -0.0076$$

$$n = 0.1595$$

3.3 LQR control and tuning

An LQR type control is utilized to optimize the performance of a closed-loop system by providing optimally tuned controller gains. LQR being a popular choice amongst AUVs, it has been employed for steering control [37] depth control [38],[39], and hovering control[40]-[42]. The gain matrix (K) is derived for USFG by utilizing the dynamic state-space model. For USFG, the state space equations (6-9) for single input multiple outputs (SIMO) systems are:

$$\frac{ds_1}{dt} = As_1 + Bj_1 \tag{9}$$

$$\frac{ds_2}{dt} = As_2 + Bj_1 \tag{10}$$

$$z_1 = Cs_1 \tag{11}$$

Accepted Manuscript Not Copyedited
Downloaded from http://asmedigitalcollection.asme.org/offshoremechanics/article-pdf/doi/10.1115/1.4056419/6954108/omae-22-1049.pdf by Stavanger University user on 07 December 2022

Journal of Offshore Mechanics and Arctic Engineering. Received March 29, 2022;
Accepted manuscript posted November 30, 2022. doi:10.1115/1.4056419
Copyright © 2022 by ASME

$$z_2 = Cs_2 \tag{12}$$

A, *B* and *C* are the state, input, and output matrices, respectively. Whereas $z_{1,2}$, are scalar matrices of the system representing output, $s_{1,2}$ are the state variables, and j_1 is the input scalar matrix. State matrices of the system (*A*, *B,* and *C*) are calculated in *Section 3.3.1*.

The control law implemented here is given by equation (10), where *K* is the gain matrix.

$$j = -K\delta s \tag{13}$$

For an optimal gain matrix for LQR, *A* and *B* matrices are obtained from the linearization of the system. This is done to reduce the cost function formed based on the control law. It relies on the summation of the square of the input variables of the system. Equation (11) gives the cost function:

$$G = \int_0^{\infty} \delta s^T Q\delta s + \delta j^T R\delta j \, dt \tag{14}$$

Here *R* is the matrix for the penalty of control cost, and Q is the penalty for state cost. The aim is to adjust *Q* and *R* to find an optimal balance between actuator effort and the system's performance. Weights of these penalty matrices are adjusted to tune the LQR controller for the desired application. This is done in *Section 3.3.2.*

3.3.1 Linearization

The model used for linearization is from work presented by Ahmad and Xing [43]. Linearization for two case studies is performed in this section, i.e., *Case 1* and *Case 2*, as

Accepted Manuscript Not Copyedited
Downloaded from http://asmedigitalcollection.asme.org/offshoremechanics/article-pdf/doi/10.1115/1.4056419/6954108/omae-22-1049.pdf by Stavanger University user on 07 December 2022

Journal of Offshore Mechanics and Arctic Engineering. Received March 29, 2022;
Accepted manuscript posted November 30, 2022. doi:10.1115/1.4056419
Copyright © 2022 by ASME

highlighted in *Section 3.4*. Previously Ahmad and Xing [1] investigated 30° and 40° glide angles for the linearization of the USFG model. As for *Case 2*, the model is linearized at a 38° gliding angle. Simulink model linearizer is used to linearize the mathematical model of the USFG at an established operational point. Open-loop inputs [ϑ; $\dot{x}$; $\dot{y}$; $\dot{\theta}$] and outputs [$\dot{\theta}$; $\ddot{x}$; $\ddot{y}$; $\ddot{\theta}$] are marked as shown in Figure *13*. This results in a 4x4 *A*, 4x1 *B,* and 2x4 *C* matrices as depicted in equation (12):

$$A = \begin{bmatrix} 0 & 0 & 0 & 1 \\ 0.4298 & -0.2032 & -0.2606 & 5.51 \times 10^{-12} \\ 0.6811 & -0.2941 & -0.4128 & 0 \\ -2.10 \times 10^{-08} & 1.12 \times 10^{-09} & 1.52 \times 10^{-09} & -3.15 \times 10^{-04} \end{bmatrix}$$

$$B = \begin{bmatrix} 0 \\ -1.58 \times 10^{-12} \\ -8.88 \times 10^{-13} \\ 2.64 \times 10^{-05} \end{bmatrix} \tag{15}$$

$$C = \begin{bmatrix} 0 & 0.7886 & -0.6149 & 0 \\ 0 & 0.4572 & -0.5863 & 0 \end{bmatrix}$$

3.3.2 Tuning of LQR

Based on the state matrices (*A*, *B,* and *C*) obtained from linearization, LQR is tuned to obtain the desired response of the glider. Tuning is done by adjusting the values (penalties) of the *Q* and *R* matrices. A complete and holistic understanding of the dynamics of the USFG is essential to tune the controller. This involves studying the response time of the system for anticipated system performance. Additionally, Bryson's technique is employed to tune the values for the USFG model. This involves fine-tuning the Q and R matrices manually according

Accepted Manuscript Not Copyedited
Downloaded from http://asmedigitalcollection.asme.org/offshoremechanics/article-pdf/doi/10.1115/1.4056419/6954108/omae-22-1049.pdf by Stavanger University user on 07 December 2022

Journal of Offshore Mechanics and Arctic Engineering. Received March 29, 2022;
Accepted manuscript posted November 30, 2022. doi:10.1115/1.4056419
Copyright © 2022 by ASME

to the final response of the glider (*Case 2: The 38° glide*). Penalty on the *R* matrix adjusts the controller effort. As for the *Q* matrix, it governs the acceptable error amongst the output variables/states. Detailed analysis for the controller tuning can be found in Ahmad and Xing [1], which also forms the basis of a good system response for this study. The Q and R matrices are presented in equation (13).

The 10^5 for the 41-coefficient represents that the acceleration in the pitch direction is penalized heavily, as the system is designed to attain a pitching angle of 38°. The gain matrix

$$Q = \begin{bmatrix} 0 \\ 0 \\ 0 \\ 10^5 \end{bmatrix} \tag{16}$$

$$R = [0.01]$$

(*K*) is presented in equation (14).

$$K = [-5.31 \times 10^{-10} \quad 2.43 \times 10^{-10} \quad 3.21 \times 10^{-10} \quad 2.58] \tag{17}$$

3.4 Controlled gliding of USFG

This section analyses two different glides of the USFG and the different characteristics of each controlled glide. The following cases are simulated.

- Case 1: Equilibrium glide
- Case 2: The 38° glide path

Accepted Manuscript Not Copyedited

Downloaded from http://asmedigitalcollection.asme.org/offshoremechanics/article-pdf/doi/10.1115/1.4056419/6954108/omae-22-1049.pdf by Stavanger University user on 07 December 2022

Journal of Offshore Mechanics and Arctic Engineering. Received March 29, 2022;
Accepted manuscript posted November 30, 2022. doi:10.1115/1.4056419
Copyright © 2022 by ASME

3.4.1 Equilibrium glide

The sawtooth path taken by the glider, as depicted in Figure *2*, is termed as an equilibrium glide or gliding path. The USFG follows this equilibrium path to extend its travel range as taking a pre-planned route may optimize the freight operations. Two equilibrium glide paths are simulated for this analysis and are presented in Figure 15. This plot represents the time series of the glider's pitch response.

For this study, the glider is programmed to follow an operating depth of 200 m while following a 38° glide angle by using two separate controllers: Proportional-integral-derivative (PID) and LQR type control. The objective of the investigation is to compare the heave response of the two different control systems against the planned path.

The tuning gains selected for this study are the most ideal for PID application, as other values increase the response time of the output. For this scenario, the glider changes the glide angle rapidly as it responds to changes in the commanded pitch. This leads to more glides/dives for a certain distance travelled, resulting in higher power consumption onboard. Overrun and overshoot can also be observed when PID is utilized to control the pitching motion of the glider. Moreover, these gains cannot be further optimized as doing so induces non-practical response times.

LQR type control enables the glider to respond to changes in operating conditions more efficiently and effectively by utilizing less actuator effort. An error of merely 3% is observed as compared to 11% for PID. With enhanced tuning, then this error can be further reduced

Accepted Manuscript Not Copyedited
Downloaded from http://asmedigitalcollection.asme.org/offshoremechanics/article-pdf/doi/10.1115/1.4056419/6954108/omae-22-1049.pdf by Stavanger University user on 07 December 2022

Journal of Offshore Mechanics and Arctic Engineering. Received March 29, 2022;
Accepted manuscript posted November 30, 2022. doi:10.1115/1.4056419
Copyright © 2022 by ASME

for LQR. Furthermore, the deviations in the upper and lower bounds are also shortened due to reduced overrun.

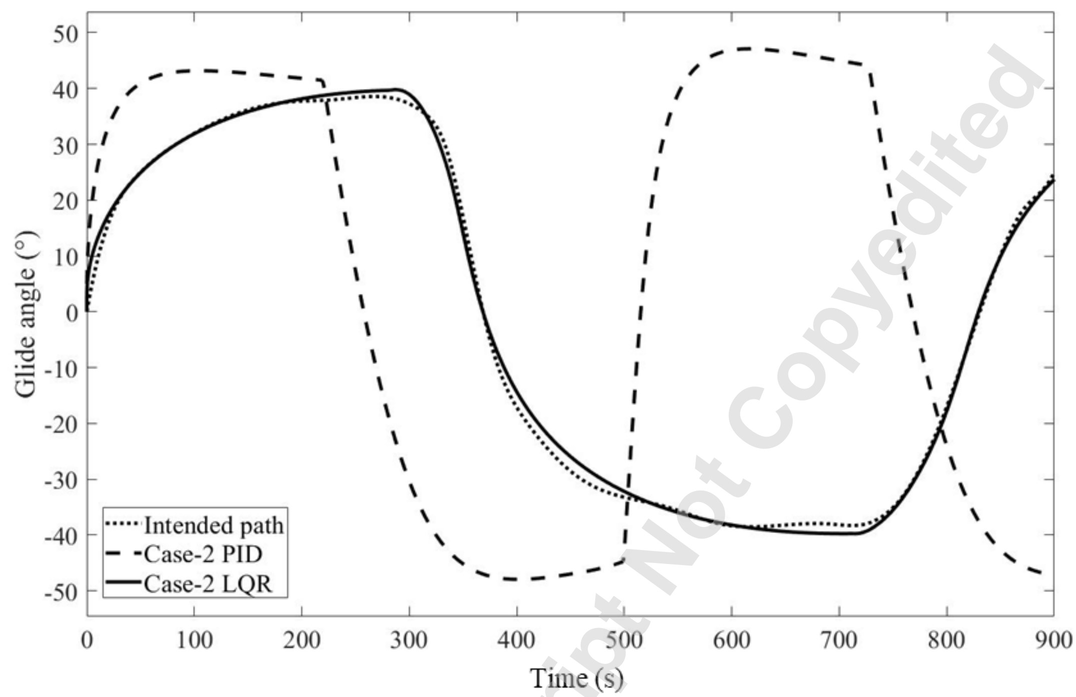

Figure 15 Equilibrium glide paths (PID vs LQR) in the vertical plane.

3.4.2 The 38° glide path

Figure 16 compares the pitch response of LQR and PID. This controlled glide of the USFG requires the glider to pitch at an angle of -38° while diving. The negative convention is to represent anti-clockwise rotation in a 2D vertical plane. Actuator effort is compared for both cases of the controller.

As illustrated in Figure 16, the PID controller fails to mitigate the noise from the output response. The oscillations in the pitch response increase the controller effort drastically. Consequently, the percentage overshoot and the signal's settling time increases significantly

Accepted Manuscript Not Copyedited
Downloaded from http://asmedigitalcollection.asme.org/offshoremechanics/article-pdf/doi/10.1115/1.4056419/6954108/omae-22-1049.pdf by Stavanger University user on 07 December 2022

Journal of Offshore Mechanics and Arctic Engineering. Received March 29, 2022;
Accepted manuscript posted November 30, 2022. doi:10.1115/1.4056419
Copyright © 2022 by ASME

to 13.5 % and 15.4 seconds correspondingly. Moreover, higher overshoot/peaks affect the USFG's dynamics negatively. As the objective of the glider is to conserve energy while transporting cargo over larger distances, so excessive actuator effort spent on course correction is not ideal for this scenario. Finally, the PID controller employed for this controlled glide is tuned aggressively. This tuning does not add value to the overall system response. Subsequently leading to no room for improvement as far as the tunning of PID is concerned. Generally, a controller ideal for such applications is the one that causes fewer oscillations while reducing the settling time.

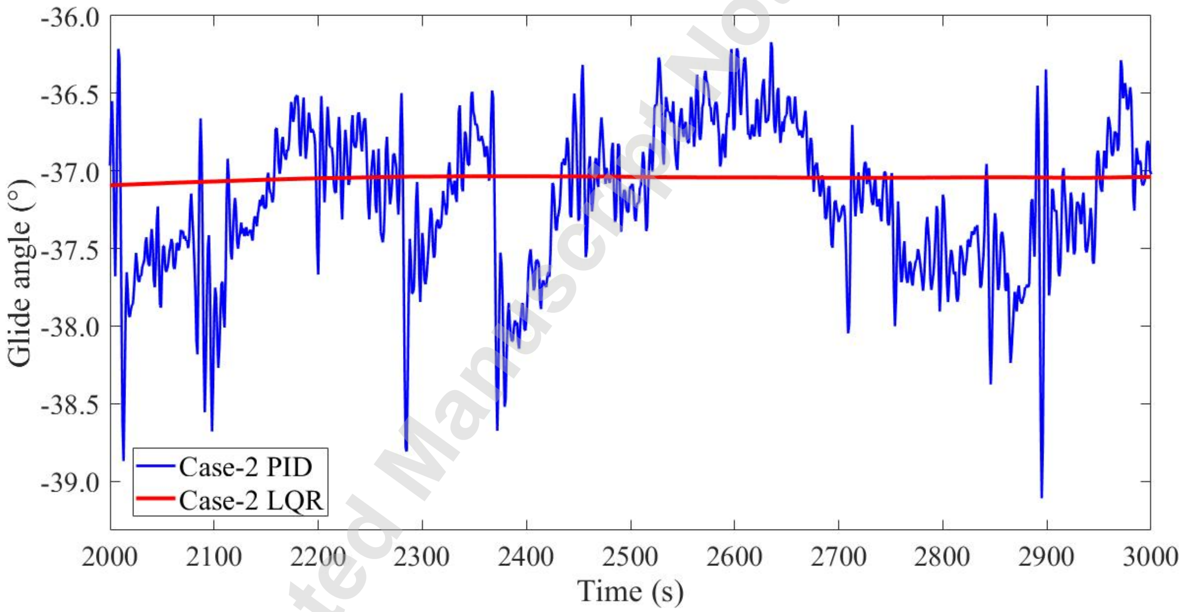

Figure 16 38° Glide path.

LQR is tuned according to the system's response to reduce the fluctuations. The controller effort is penalized lightly in the R matrix, as indicated in equation (13). This induces the controller to respond quickly following the desired steered command while decreasing the

Accepted Manuscript Not Copyedited
Downloaded from http://asmedigitalcollection.asme.org/offshoremechanics/article-pdf/doi/10.1115/1.4056419/6954108/omae-22-1049.pdf by Stavanger University user on 07 December 2022

Journal of Offshore Mechanics and Arctic Engineering. Received March 29, 2022;
Accepted manuscript posted November 30, 2022. doi:10.1115/1.4056419
Copyright © 2022 by ASME

rise and settling time significantly. A downside of these gains is that the slope of the output signal increases slightly, but a comprise can be made for this application, as it is not of much concern for this analysis. The system becomes robust when an LQR-type control is utilized as the gains selected for this scenario are ideal compared to their counterparts. Moreover, in this case, the controller gains can be further optimized to get the desired characteristics, unlike for the PID controller.

4 CONCLUSIONS

In this paper, the baseline design of USFG is presented, consisting of a mechanical design and the control design. The final derived design is presented in Table 9. The control design consists of the manoeuvring model along with 2 case studies. The USFG aims to carry CO_2 for injection to the well sites, though reducing the overall carbon footprint of the freight industry. The baseline design of the USFG is developed to promote research in underwater cargo-carrying vessels while also serving as a potential replacement for conventional transport methods, i.e., pipelines and tankers. The main details of the design are presented in the first part of the work. The distinguishing feature of the USFG is its dual hull/shell design which utilizes an ACPS to reduce the overall structural weight. As for the second part, an extensive analysis is presented, which highlights the major differences between LQR and PID type controllers used for autonomous naval applications. LQR is preferred for both cases of the controlled glides, as it reduces oscillations while enhancing the system's robustness. Finally, the tuning method of LQR is

Accepted Manuscript Not Copyedited
Downloaded from http://asmedigitalcollection.asme.org/offshoremechanics/article-pdf/doi/10.1115/1.4056419/6954108/omae-22-1049.pdf by Stavanger University user on 07 December 2022

Journal of Offshore Mechanics and Arctic Engineering. Received March 29, 2022;
Accepted manuscript posted November 30, 2022. doi:10.1115/1.4056419
Copyright © 2022 by ASME

straightforward compared to the conventional PID control that requires unwarranted tunning and computational power for results to be converged.

Table 9 Design summary of USFG.

Vessel Features	Value
Length [m]	50.25
Beam [m]	5.5
Total power consumptions [kW]	8
Range [km]	400
Speed [knots]	2
Lightweight [ton]	495
Deadweight [ton]	531
Displacement [ton]	1026
Lightweight [m^3]	483
Deadweight [m^3]	518
Displacement [m^3]	1001

Appendix A. Calculation of reference wing area

The hydrofoils reference area of 5 m^2 is derived based on Graver's work [35]. Following parameters are used in the calculation of wing area.

Accepted Manuscript Not Copyedited
Downloaded from http://asmedigitalcollection.asme.org/offshoremechanics/article-pdf/doi/10.1115/1.4056419/6954108/omae-22-1049.pdf by Stavanger University user on 07 December 2022

Journal of Offshore Mechanics and Arctic Engineering. Received March 29, 2022;
Accepted manuscript posted November 30, 2022. doi:10.1115/1.4056419
Copyright © 2022 by ASME

- ***D_{ton}***: described as DWT valued at 531 tons, is the amount of freight or cargo (CO_2 for this paper) that the USFG can transport.
- ***H***: defined as nominal operating depth, which is estimated to be 200 m.
- ***BF***: ballast fraction of 0.15% is preferred.
- ***ξ***: the gliding angle of 30º is selected to conserve power while gliding at a constant speed.

The hydrofoil area can be calculated from these expressions:

$$BF = \frac{m_o}{D_{ton} \times 1000} \tag{18}$$

$$S = \sqrt[2]{\left(\frac{m_o \times g \times \sin\xi}{0.5 \times \rho_w \times C_{DVol} \times Vol^{\frac{2}{3}}}\right)} \tag{19}$$

$$S_x = S \times \cos\xi \tag{20}$$

$$D_{force} = S^2 \times 0.5 \times \rho_w \times C_{DVol} \times Vol^{\frac{2}{3}} \tag{21}$$

$$L_{force} = \frac{D_{force}}{\tan\xi} \tag{22}$$

Accepted Manuscript Not Copyedited
Downloaded from http://asmedigitalcollection.asme.org/offshoremechanics/article-pdf/doi/10.1115/1.4056419/6954108/omae-22-1049.pdf by Stavanger University user on 07 December 2022

Journal of Offshore Mechanics and Arctic Engineering. Received March 29, 2022;
Accepted manuscript posted November 30, 2022. doi:10.1115/1.4056419
Copyright © 2022 by ASME

$$A_{reference} = \frac{L}{S^2 \times 0.5 \times \rho_w \times C_L} \tag{23}$$

Where m_o is the mass of the USFG, S is the velocity of the glider, g is the gravitational constant, ρ_w is the density of water, C_{DVol} and C_L is the volumetric drag and lift coefficient of the USFG, Vol is the entire volume of the USFG, and L_{force} and D_{force} are the lift and drag forces, respectively.

The drag force is calculated to be 3907 Newtons, whereas the lift force comes out to be 6767 Newtons for this case. It must be noted that the USFG attains a total horizontal speed of 1 m/s for these conditions.

Accepted Manuscript Not Copyedited

Downloaded from http://asmedigitalcollection.asme.org/offshoremechanics/article-pdf/doi/10.1115/1.4056419/6954108/omae-22-1049.pdf by Stavanger University user on 07 December 2022

Journal of Offshore Mechanics and Arctic Engineering. Received March 29, 2022;
Accepted manuscript posted November 30, 2022. doi:10.1115/1.4056419
Copyright © 2022 by ASME

627 **NOMENCLATURE**

USFG	UiS subsea-freight glider
CCS	Carbon capture and storage
DWT	Dead-weight tonnage
SST	Subsea shuttle tanker
AUVs	Autonomous Underwater Vehicles
PID	Proportional-integral-derivative
ASME BPVC	American Society of Mechanical Engineers Boilers and Pressure Vessel Code
DNVGL-RU-NAVAL-Pt4Ch1	DNVGL Rules for Classification for Naval Vessels, Part 4 Sub-surface ships, Section 1 Submarine
GM	Metacentric height
G	Centre of gravity
B	Centre of buoyancy
LQR	Linear-quadratic regulator
K	Gain matrix
2D	Two-dimensional
M_e	External pitch moment
Z_e	Force in heave direction
X_e	Force in surge direction
SIMO	Single input multiple outputs
A, B, and C	State space matrices

628

629

Accepted Manuscript Not Copyedited

Downloaded from http://asmedigitalcollection.asme.org/offshoremechanics/article-pdf/doi/10.1115/1.4056419/6954108/omae-22-1049.pdf by Stavanger University user on 07 December 2022

Journal of Offshore Mechanics and Arctic Engineering. Received March 29, 2022;
Accepted manuscript posted November 30, 2022. doi:10.1115/1.4056419
Copyright © 2022 by ASME

5 REFERENCES

[1] R. FULLENBAUM, J. FALLON, and B. FLANAGAN, "Oil & Natural Gas Transportation & Storage Infrastructure: Status, Trends, & Economic Benefits," IHS Global Inc., 2013. [Online]. Available: https://www.circleofblue.org/wp-content/uploads/2014/12/API-Infrastructure-Investment-Study.pdf.

[2] A. C. Palmer and R. A. King, Subsea pipeline engineering, 2nd ed. Tulsa, Okla: PennWell, 2008.

[3] C. Vestereng. "Shuttle tankers in Brazil." DNV-Maritime Impact. https://www.dnv.com/expert-story/maritime-impact/shuttle-tankers-Brazil.html (accessed 30 January 2022).

[4] J. Wilson, "Shuttle tankers vs pipelines in the GOM frontier," World oil, vol. 229, no. 4, pp. 149-151, 2008.

[5] Y. Xing, "A conceptual large autonomous subsea freight-glider for liquid CO2 transportation," in International Conference on Offshore Mechanics and Arctic Engineering, 2021, vol. 85161: American Society of Mechanical Engineers, p. V006T06A052.

[6] Xing, Y. (2021) Burst Pressure Capacity of the Cargo Tanks used in a Novel Large Subsea Freight-Glider, Third Conference of Computational Methods in Offshore Technology, Stavanger, Norway.

[7] Y. Xing, T. A. D. Santoso, and Y. Ma, "Technical–Economic Feasibility Analysis of Subsea Shuttle Tanker," Journal of Marine Science and Engineering, vol. 10, no. 1, p. 20, 2021.

[8] H. Stommel, "The Slocum mission," Oceanography, vol. 2, no. 1, pp. 22-25, 1989.

Accepted Manuscript Not Copyedited

Downloaded from http://asmedigitalcollection.asme.org/offshoremechanics/article-pdf/doi/10.1115/1.4056419/6954108/omae-22-1049.pdf by Stavanger University user on 07 December 2022

Journal of Offshore Mechanics and Arctic Engineering. Received March 29, 2022;
Accepted manuscript posted November 30, 2022. doi:10.1115/1.4056419
Copyright © 2022 by ASME

[9] Evo Logics. "Evo Logics BOSS - Manta Ray." https://evologics.de/projects/boss (accessed 31 January 2022).

[10] DOF Subsea. "Glider AUV." https://www.dofsubsea.com/rov/glider-auv/ (accessed 31 January 2022).

[11] P. Taylor and J. Montgomery, "Arctic submarine tanker system," in Offshore Technology Conference, 1977: OnePetro.

[12] L. R. Jacobsen, "Subsea Transport of Arctic Oil-A Technical and Economic Evaluation," in Offshore Technology Conference, 1971: OnePetro.

[13] L. Jacobsen, K. Lawrence, K. Hall, P. Canning, and E. Gardner, "Transportation of LNG from the Arctic by commercial submarine," Marine Technology and SNAME News, vol. 20, no. 04, pp. 377-384, 1983.

[14] G. Griffiths, Technology and applications of autonomous underwater vehicles. CRC Press, 2002.

[15] Equinor Energy AS. RD662093 Subsea Shuttle System, 2019.

[16] K.E. Ellingsen, O. Ravndal, L. Reinas, J.H. Hansen, F. Marra, E. Myhre and k. Sveberg, RD677082 Subsea Shuttle System, 2020.

[17] Jamissen, P.L., Ma, Y. and Xing, Y.* (2022) Probabilistic design of thin-walled cylindrical hull structures for application in large cargo submarines, International Conference on Ocean, Offshore and Artic Engineering, Hamburg, Germany.

[18] Xing, Y., Janocha, M.J., Yin, G. and Ong, M.C. (2022) CFD investigation on hydrodynamic resistance of a novel subsea shuttle tanker, Journal of Marine Science and Engineering 9(12), 1411

Accepted Manuscript Not Copyedited

Downloaded from http://asmedigitalcollection.asme.org/offshoremechanics/article-pdf/doi/10.1115/1.4056419/6954108/omae-22-1049.pdf by Stavanger University user on 07 December 2022

Journal of Offshore Mechanics and Arctic Engineering. Received March 29, 2022;
Accepted manuscript posted November 30, 2022. doi:10.1115/1.4056419
Copyright © 2022 by ASME

[19] Y. Xing, M. C. Ong, T. Hemmingsen, K. E. Ellingsen, and L. Reinås, "Design considerations of a subsea shuttle tanker system for liquid carbon dioxide transportation," Journal of Offshore Mechanics and Arctic Engineering, vol. 143, no. 4, 2021.

[20] Y. Ma, Y. Xing, M. C. Ong, and T. H. Hemmingsen, "Baseline design of a subsea shuttle tanker system for liquid carbon dioxide transportation," Ocean Engineering, vol. 240, p. 109891, 2021.

[21] Y. Ma, D. Sui, Y. Xing, M.C. Ong and T.H. Hemmingsen (2021) Depth Control Modelling and Analysis of a Subsea Shuttle Tanker, International Conference on Ocean, Offshore and Artic Engineering, Virtual, Online.

[22] J. W. Bahlman, S. M. Swartz, D. K. Riskin, and K. S. Breuer, "Glide performance and aerodynamics of non-equilibrium glides in northern flying squirrels (Glaucomys sabrinus)," (in eng), J R Soc Interface, vol. 10, no. 80, pp. 20120794-20120794, 2012, DOI: 10.1098/rsif.2012.0794.

[23] Norwegian Petroleum Directorate (NPD). "Carbon Capture and Storage." http://www.norskpetroleum.no/en/environment-and-technology/carbon-capture-and-storage (accessed 1 February 2022).

[24] Equinor. "Northern Lights CC." https://www.equinor.com/en/what-we-do/northern-lights.html (accessed 1 February 2022).

[25] P. Taylor, "Energy Technology Perspectives," International Energy Agency, 2010.

[26] A. Papanikolaou, Ship design: methodologies of preliminary design. Springer, 2014.

[27] Carbon Capture Storage, and Association. "What Is CCS?" http://www.ccsassociation.org/what-is-ccs/ (accessed 2 February 2022).

Accepted Manuscript Not Copyedited
Downloaded from http://asmedigitalcollection.asme.org/offshoremechanics/article-pdf/doi/10.1115/1.4056419/6954108/omae-22-1049.pdf by Stavanger University user on 07 December 2022

Journal of Offshore Mechanics and Arctic Engineering. Received March 29, 2022;
Accepted manuscript posted November 30, 2022. doi:10.1115/1.4056419
Copyright © 2022 by ASME

[28] ASME. Boiler and Pressure Vessel Code, Section VIII, Division 2; The American Society of Mechanical Engineers: New York, NY, USA, 2015.

[29] DNV-GL Rules for Classification, Naval Vessels, Part 4 Sub-Surface Ships. Available online: https://rules.dnv.com/docs/pdf/DNV/RU-NAVAL/2018-01/DNVGL-RU-NAVAL-Pt4Ch1.pdf (accessed on 4 February 2022).

[30] National Centers for Environmental, and Information (NCEI). "Greenland, Iceland, and Norwegian Seas Regional Climatology." https://www.ncei.noaa.gov/products/greenland-iceland-and-norwegian-seas-regional-climatology (accessed 7 February 2022).

[31] P. Klis, S. Wang S and Y. Xing. Technical and Economic Feasibility Analysis of a Conceptual Subsea Freight Glider for CO2 Transportation. Journal of Marine Science and Engineering. 2022; 10(8):1108. https://doi.org/10.3390/jmse10081108

[32] A. Mariano, E. Ryan, B. Perkins, and S. Smithers, "The Mariano Global Surface Velocity Analysis 1.0," p. 61, 07/01 1995.

[33] G. Ersdal, "An overview of ocean currents with emphasis on currents on the Norwegian continental shelf," 2001.

[34] R. Sætre, The Norwegian coastal current: oceanography and climate. Akademika Pub, 2007.

[35] Tools, A. NACA 4412 (naca4412-il). http://airfoiltools.com/airfoil/details?airfoil=naca4412-il

[36] J. G. Graver, "Underwater gliders: Dynamics, control and design," 2005.

[37] Bae, S. B. Shin, D. H. Kwon, S. T. Joo, and M. G, "An LQR controller for autonomous underwater vehicle," Journal of Institute of Control, Robotics and Systems, vol. 20, no. 2, pp. 132-137, 2014.

Accepted Manuscript Not Copyedited

Downloaded from http://asmedigitalcollection.asme.org/offshoremechanics/article-pdf/doi/10.1115/1.4056419/6954108/omae-22-1049.pdf by Stavanger University user on 07 December 2022

Journal of Offshore Mechanics and Arctic Engineering. Received March 29, 2022;
Accepted manuscript posted November 30, 2022. doi:10.1115/1.4056419
Copyright © 2022 by ASME

[38] P. Burlacu, V. Dobref, N. Badara, and O. Tarabuta, "A LQR controller for an AUV depth control," Annals of DAAAM & Proceedings, pp. 125-127, 2007.

[39] U.N. Ahmad, Y. Xing and S. Wang. (2022). Determination of extreme responses of USFG's equilibrium glide path hovering in ocean current, accepted in Ocean Engineering.

[40] Y. Ma, Y. Xing and D. Sui (2022). "Trajectory Envelope of a Subsea Shuttle Tanker Hovering in Stochastic Ocean Current - Model Development and Tuning." ASME. J. Offshore Mech. Arct. Eng.

[41] Y. Xing, O. Gaidai, Y. Ma, A. Naess and F. Wang (2022) A novel design approach for estimation of extreme responses of a subsea shuttle tanker hovering in ocean current considering aft thruster failure, Applied Ocean Research 123, 103197.

[42] O. Gaidai, Y. Xing, and R. Balakrishna (2022) Improving extreme response prediction of a subsea shuttle tanker hovering in ocean current using an alternative highly correlated response signal, accepted in Results in Engineering.

[43] U. Ahmad and Y. Xing, "A 2D model for the study of equilibrium glide paths of UiS Subsea Freight-Glider," in IOP Conference Series: Materials Science and Engineering, 2021, vol. 1201, no. 1: IOP Publishing, p. 012022.

[44]U. Ahmad and Y. Xing, "UIS Subsea Freight Glider: controller design and analysis," in International Conference on Offshore Mechanics and Arctic Engineering, 2022, American Society of Mechanical Engineers.

Accepted Manuscript Not Copyedited

Downloaded from http://asmedigitalcollection.asme.org/offshoremechanics/article-pdf/doi/10.1115/1.4056419/6954108/omae-22-1049.pdf by Stavanger University user on 07 December 2022

Journal of Offshore Mechanics and Arctic Engineering. Received March 29, 2022;
Accepted manuscript posted November 30, 2022. doi:10.1115/1.4056419
Copyright © 2022 by ASME

Figure Captions List

Fig. 1 Illustration of UiS subsea-freight glider.

Fig. 2 Equilibrium glide paths.

Fig. 3 Ballasting system for USFG – top view of the glider.

Fig. 4 Marine CCS process utilizing USFG.

Fig. 5 Norwegian sector storage sites for the CCS projects [20].

Fig. 6 Design flow for USFG baseline design.

Fig. 7 CCS sites depth with USFG depth definitions [20].

Fig. 8 USFG's general arrangement.

Fig. 9 USFG's global parameters.

Fig. 10 USFG's gliding parameters – side view of the glider.

Fig. 11 Horizontal velocity vs power consumption.

Fig. 12 Coordinate system.

Fig. 13 Mathematical model of the USFG.

Fig. 14 Simulink plant model - Lift and drag forces, ballast system, and USFG.

Fig. 15 Equilibrium glide paths (PID vs LQR) in the vertical plane.

Fig. 16 38° Glide path.

Accepted Manuscript Not Copyedited

Downloaded from http://asmedigitalcollection.asme.org/offshoremechanics/article-pdf/doi/10.1115/1.4056419/6954108/omae-22-1049.pdf by Stavanger University user on 07 December 2022

Journal of Offshore Mechanics and Arctic Engineering. Received March 29, 2022;
Accepted manuscript posted November 30, 2022. doi:10.1115/1.4056419
Copyright © 2022 by ASME

Table Caption List

Accepted Manuscript Not Copyedited

Downloaded from http://asmedigitalcollection.asme.org/offshoremechanics/article-pdf/doi/10.1115/1.4056419/6954108/omae-22-1049.pdf by Stavanger University user on 07 December 2022